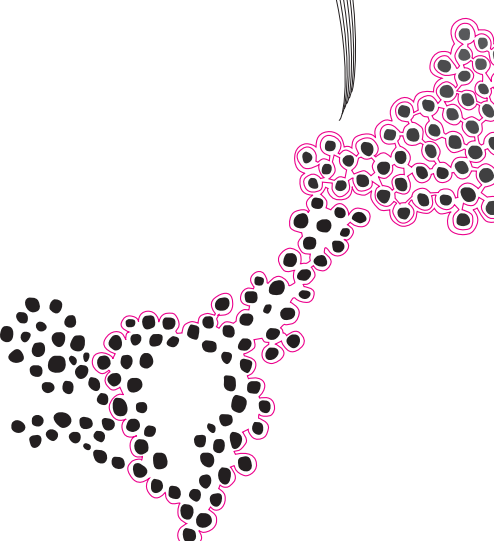




MSc Thesis Mechanical Engineering

A comparative study of
bio-inspired dual reciprocating
drilling as opposed to
conventional rotary drilling
methods using Discrete
Element Method (DEM)
simulations

Ana Vukasovic



Supervisor: Graduation committee:
Prof.Dr.Ir M.B. de Rooij - chairman
Dr. T. Mishra - supervisor
Dr. I. Ostanin - external member

October 25, 2024

Department of Surface Technology and Tribology
Faculty of Engineering Technology,
Mechanical Engineering,
University of Twente

Acknowledgments

I want to thank my supervisors, Prof. Dr. Ir. Matthijn de Rooij and Dr. Tanmaya Mishra for their guidance with this research. A special thanks to Malek Jaran for his programming support and to Robert Jan Meijer for his help with the experiments. I also want to thank Dr. Igor Ostanin for agreeing to be a part of the graduation committee as an external member. Finally, I would like to thank my family, my partner, and my friends for their immense support and encouragement during my research.

Abstract

This thesis compares the effectiveness of reciprocating drilling and conventional rotational drilling, with a focus on the potential advantages of bio-inspired drilling technologies. By integrating experimental data and numerical simulations using the Discrete Element Method (DEM), the study analyzes how these drilling techniques perform under a variety of conditions and identifies key factors influencing their performance. The research aims to address the gap in understanding the mechanical behaviors of different drilling mechanisms and to assess the potential of reciprocating drilling for industrial applications. Initial experimental validation for different cases of simulations of linear penetration with and without rotation and with different drill bit geometries was performed due to limitations in conducting dual reciprocating drilling experiments. The validation of penetration forces showed less than a 15% discrepancy between experimental and simulated results. The initial experimental studies show that rotational drilling reduces the penetration force compared to simple penetration, while the presence of moisture in the granular substrate increases it. A sensitivity study was performed with the numerical model to explore the effects of friction, particle size, and speed on normal penetration forces, demonstrating the complexity of granular substrate behavior during drilling.

A key innovation in this study is the development of a model capable of simulating dual reciprocating motion, which was used to compare normal forces generated by three drilling methods: penetrative, rotational, and reciprocating. The findings show that reciprocating drilling mostly outperforms rotational drilling in terms of lower maximum normal penetration force, especially when operated within an optimal frequency range of 25-35 Hz. Beyond this range, the advantages of reciprocation diminish, suggesting that operational parameters play a critical role in maximizing the performance of this technique. In this study, the power consumption of the drill bit, contact forces between the substrate particles, and the granular system's coordination number were studied between different drilling methods to further discuss the drilling performance of reciprocating drilling. While we mainly compare the normal forces related to penetration, the study emphasizes that normal force is only one aspect of drilling performance. Other critical parameters, such as material removal rates, tool wear, and failure modes, require further investigation to fully assess the advantages of this method. This research provides a robust foundation for the development and optimization of bio-inspired drilling technologies, offering significant potential to improve the efficiency of drilling operations, reduce tool wear, and minimize environmental impact. In conclusion, this thesis advances the understanding of reciprocating drilling mechanisms and highlights their potential to revolutionize drilling processes through enhanced efficiency, precision, and sustainability.

Keywords: DEM, Dual reciprocating drilling, Biomimicry, YADE, Conventional drilling, Comparative analysis of drilling methods

Contents

1	Introduction	3
1.1	Background and motivation	3
1.2	Problem description	4
1.3	Research gap and relevance	5
1.4	Research question	6
1.5	Research aims and method	6
2	Literature study	7
2.1	Conventional drilling	7
2.2	Drilling and contact mechanics	8
2.2.1	Material properties	9
2.2.2	Normal contacts and Hertzian contact theory	10
2.2.3	Friction in sliding contacts	11
2.2.4	Theory of adhesive contacts	12
2.2.5	Capillarity	13
2.3	Biomimicry in drilling	14
2.3.1	Drilling in the animal kingdom	14
2.3.2	The wood wasp drilling mechanism	14
2.3.3	Numerical and experimental advances in DRD research	15
2.4	Use of simulations in drilling	16
2.5	Discrete Element Method - DEM	17
2.5.1	Working principles	17
2.6	YADE software	19
2.6.1	Contact laws	20
2.6.2	Engines	21
2.6.3	Particle representation	22
2.6.4	Contact detection and resolution	22
2.6.5	Material models	23
2.6.6	Optimizing computational time	23
2.7	Simulation stability and coordination number	24
2.8	Contact force distribution	25
3	Experimental study	26
3.1	Experiment background	26
3.2	Experiment method	27
3.2.1	Experiment setup	27
3.2.2	Procedure	28
3.3	Experiment results and limitations	29
3.3.1	Experiment 1 - Penetration test at different penetration speeds	29
3.3.2	Experiment 2 - Rotation test at different combinations of penetration and rotation speeds	31
3.3.3	Experiment 3 - Penetration test with the presence of water	33
4	Numerical modelling of drilling	36
4.1	Model setup	36
4.2	Sensitivity study	38
4.2.1	Particle size	38
4.2.2	Elastic modulus	39
4.2.3	Coefficient of friction	40
4.2.4	Penetration speed	40
4.3	Simulation validation	41
4.4	Parametric study	43
4.4.1	Modelling dual reciprocation	43
4.4.2	Effects of adhesion and partially saturated substate	44
5	Results and discussion	46
5.1	Comparing different drilling methods	46

5.2	Power analysis	48
5.3	Substrate particle contact force distribution analysis	50
5.4	Coordination number analysis	52
5.5	Modelling limitations and challenges	53
6	Conclusion and recommendation	55
6.1	Conclusion	55
6.2	Recommendation	56

1 Introduction

1.1 Background and motivation

In 1845 an Englishman Robert Beart [9] stood at the forefront of the Industrial Revolution with his invention of the rotary drilling machine. This tool represented a pinnacle of hundreds of years of evolution of ancient Chinese drilling techniques, which included spring-pole and percussion drilling, where bamboo poles or heavy iron bits were repeatedly driven into the ground and manually rotated to extract water, salt, and natural gas [22], and has continued to evolve ever since as the front-runner of the American oil boom. Rotational drilling has since held a monopoly over natural resource extraction, and following the shift to renewable energy sources, it has remained a preferred method of drilling for wind turbine installations, followed by a close second-percussive drilling. The conventional paradigm of rotational drilling has been the cornerstone of drilling operations for decades in various industries, involving the rotation of a drill bit to penetrate subsurface formations ranging from soil to metal. The drill bit rotates on its axis, applying torque to penetrate the material, while the drilling fluid is circulated to cool the bit, carry away cuttings, and maintain stability, ensuring efficient and precise excavation in mechanical operations [31]. While praised for its speed and precision, this method faces challenges such as energy inefficiency, tool wear, and limited adaptability to diverse geological conditions [11]. In response to these challenges, bio-inspired reciprocating drilling emerges as a promising alternative, drawing inspiration from nature’s ingenious mechanisms. Biological entities, such as different species of insects, have evolved efficient reciprocating drilling strategies, showcasing the potential for innovative solutions in engineering applications.

Known for its ability to bore into hardwood with remarkable efficiency, the wood wasp employs a unique reciprocating motion that allows it to penetrate tough materials effectively. This intricate drilling strategy involves the repeated insertion and retraction of its ovipositor, which mimics a reciprocating drill bit. The wood wasp’s adaptation showcases an innate ability to optimize drilling performance by minimizing energy expenditure and maximizing precision (Figure 1). This reciprocating motion aids in efficient drilling by reducing friction and preventing bit clogging [17]. Mimicking nature’s optimized drilling mechanisms would allow for penetrating various materials with minimal energy expenditure.

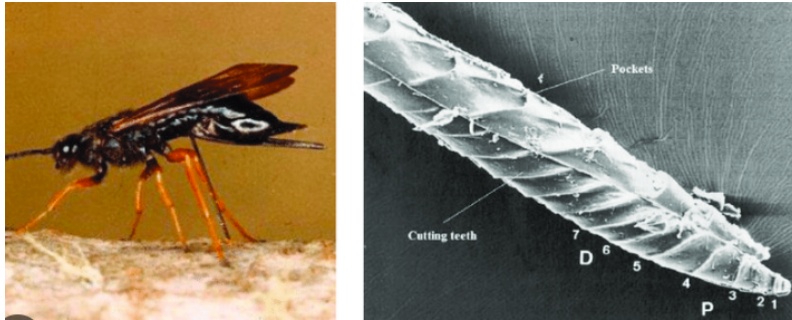


Figure 1: Wood wasp’s drilling mechanism [17]

However, despite the effectiveness of reciprocating drilling observed in nature, there is a lack of extensive experimental research data to effectively compare this method with its conventional counterparts. This thesis investigates the effectiveness of bio-inspired dual reciprocating drilling and compares it with the conventional approach of rotational drilling in order to bridge this knowledge gap. By employing advanced Discrete Element Method (DEM) simulations, the research aims to understand the mechanics related to reciprocating and rotational drilling and discern their respective advantages and limitations. Deploying DEM simulations allows a meticulous examination of the drilling process, offering insights into the fundamental mechanics at the grain and contact scale for each method. As industries strive for sustainability and technological breakthroughs, this research serves as a valuable contribution by providing a clearer understanding of the bio-inspired reciprocating drilling paradigm. The outcomes of this comparative study have the potential to guide future advancements in drilling technologies, offering environmentally conscious and efficient alternatives to conventional methods.

1.2 Problem description

As previously mentioned, conventional drilling methods face challenges regarding efficiency, wear, and geological adaptability. Additionally, they are known to be destructive due to high subsurface disturbances which are often found in raw resource mining, where large underground structures would collapse [1]. On the other hand, rotational drills were often found to exert an inadequate amount of normal force on the substrate and require substantial lubrication to facilitate the motion, causing the drilling to become unsuccessful in harder and dryer terrains [11]. Unlike rotational drilling, which relies solely on the continuous rotation of the drill bit, reciprocating drilling involves a back-and-forth oscillating motion of the drilling apparatus. This reciprocating motion enables the drill bit to exert force with less disturbance to its surroundings. A great problem of rotational drilling is the high rates of material wear and energy requirements. In the example of the wood wasp, it is demonstrated that such a small insect is able to penetrate a hard surface of the wood with no damage to its ovipositor after repeated use. This effectiveness in drilling can potentially be related to the way it approaches drilling, using dual reciprocation.

Similarly, a NASA Insight project ran into a problem when the probe got stuck in dry Martian terrain while tracking seismic activity (Figure 2) [35]. The probe had to reach a certain depth to properly carry out analyses, but this was not possible due to harsh soil conditions. This has opened the question of whether different approaches to drilling, that are specific to different substrates, could prevent this issue from happening in future missions, as developing more powerful rotary drills greatly increases the size and weight that needs to be launched into space. Dual reciprocation is an interesting topic to investigate in this context, as its unique motion could help reduce the risk of seizing the drill bit in high frictional soil or due to overheating in dry conditions.

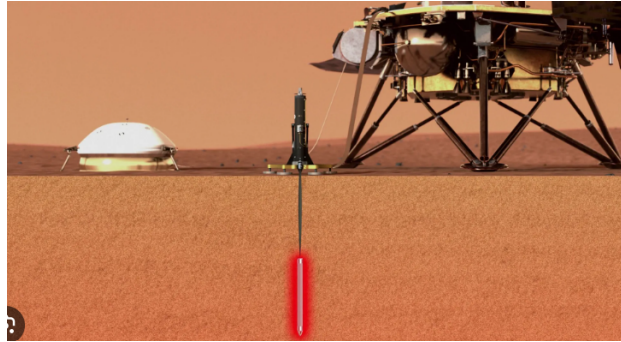


Figure 2: Insight probe [35]

As the world increasingly turns towards renewable energy sources, such as wind turbines and electric vehicles, it's crucial to acknowledge their potential adverse effects on the environment. Wind turbine installation can have devastating effects on oceanic ecosystems. The current methods employed for drilling during wind turbine installation generate substantial underwater noise, which can disrupt the sensitive echo-location mechanisms relied upon by numerous marine species for communication, navigation, and locating prey or mates. This disruption can extend for significant distances around the construction site, impacting a wide range of marine life [7]. Furthermore, the installation process itself can trigger secondary effects, such as earthquakes, with profound consequences for ocean habitats. There have been instances where the installation activities have induced small earthquakes, particularly in regions with unstable underwater geological formations. These seismic events can, in turn, trigger underwater landslides, leading to the destruction of habitats for marine life over extensive areas. Such disturbances can have long-lasting repercussions on marine ecosystems, affecting species diversity, population dynamics, and overall ecosystem health [14]. A similar trend can be observed with the mining of rare minerals needed for Lithium-ion battery production in the electric vehicle industry. High levels of vibration increase the risk of drilling near unstable geological formations and the high energy requirements make this method less cost-effective. These issues highlight the need for innovative drilling methods that will reduce noise pollution and the occurrence and effect of seismic disturbances.

It becomes apparent that less harmful and more efficient drilling methods are necessary to fully embrace the era of sustainability, which is why the Surface Technology and Tribology group at the

University of Twente has invested in a bio-inspired drill. This research culminated in the development of the reciprocating drill prototype inspired by the aforementioned wood wasp’s ovipositor, which was built as a proof-of-concept. The main use of this tool is to experimentally analyze the effectiveness of reciprocating drilling. A 3D-printed conical drill bit is split into two halves which are connected to a guiding mechanism that allows for the reciprocating motion, another guiding mechanism is present to move the drill bit vertically. The system is run by a geared DC electric motor with the power and torque ratings of 80W and 1.1 Nm respectively. The setup is shown in Figure 3a below, with a simplified view presented in Figure 3b.

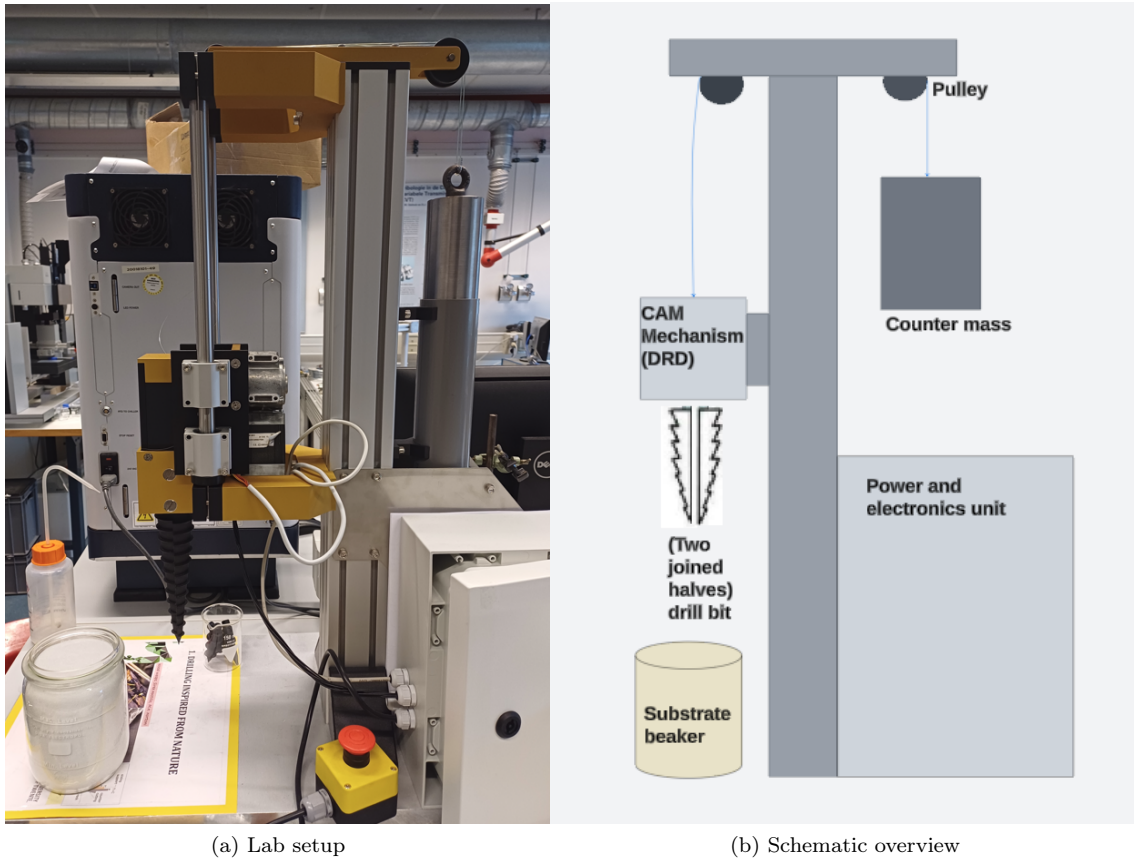


Figure 3: Drill-bug prototype

1.3 Research gap and relevance

Despite its potential, a comprehensive understanding of the comparative advantages and limitations between bio-inspired reciprocating drilling and conventional rotational drilling is lacking in recent literature. Additionally, as will be discussed in further chapters, the prototype itself has many limitations (such as the lack of a data acquisition setup or sensor data) that hinder the advancements in reciprocating drilling research at the University of Twente specifically, pushing the need for rapid and adaptive research through the medium of DEM simulations. This knowledge gap hinders the industry’s ability to make informed decisions regarding the adoption of more efficient and environmentally friendly drilling technologies, which is why a comparative study between the two drilling methods is necessary moving forward.

The wood wasp’s adaptations for drilling show great potential to solve many issues currently faced by conventional drilling methods, however, there is still a lot to explore when it comes to gathering and analyzing dual-reciprocation drilling data. There is a need for further exploration of drilling with dual reciprocation and its potential use in industrial drilling scenarios. Furthermore, experiments and numerical studies that compare DRD to conventional types of drilling are necessary in order to establish DRD as a strong contestant to currently used drilling methods. There are

many disadvantages of conventional drilling methodologies which increase the urgency for more innovative drilling technology to reduce the environmental footprint of drilling operations and to facilitate better drilling operations in more challenging terrains. Better drilling options would reduce operational costs, extend tool life due to lower wear and tear, and minimize damage to the environment. In the following chapter, a comprehensive literature study is carried out to explain the most important concepts in drilling, contact mechanics, and DEM theory. This study will also highlight the lack of DRD simulations and experiments that directly compare the performance of DRD to conventional drilling methods within the context of drilling for resources. Hence, this gap is the main focus of this study.

1.4 Research question

As mentioned earlier, to further analyze the suitability of dual reciprocating drilling for industrial purposes, there needs to be a comparison made with the current method of choice: rotational drilling. A research question: *Is reciprocating drilling more effective than conventional rotational drilling?* is formulated to guide this research to bridge the previously defined knowledge gap, and give an answer to whether DRD is a suitable rival for rotational drilling in different industrial processes.

To further guide this research, the following sub-questions were defined:

- a.) *Can the DEM simulation be validated against simple penetration experiments?*
- b.) *Can DEM be used to model the reciprocating drilling motions?*
- c.) *Can the penetration force of different drilling methods be compared?*

1.5 Research aims and method

The aim of this thesis is to *analyze whether conventional drilling methods (mainly rotational drilling) can be outperformed by dual reciprocating drilling in certain conditions, in terms of reducing the forces exerted on the drill bit during penetration.* The two drilling methods will be directly compared, and more information will be derived on whether reciprocation shows any signs of easier substrate penetration. This aim will be realized through a set of objectives defined below:

- Produce a numerical model describing rotational drilling, as well as a model showing dual reciprocating drilling using DEM.
- Analyze and model drill bit-substrate interactions in both rotating and reciprocating drilling using DEM simulations.
- Quantify the maximum normal force exerted during drilling to compare different methods.

To achieve these objectives, the following method will be executed throughout this study:

- Develop and conduct drilling experiments to measure normal forces during penetrative and rotating drilling.
- Develop a scaled-down prototype model of the penetrative and rotating drilling setup and run sensitivity studies to test the model's integrity.
- Run full-scale simulations and compare simulation results with experimental data to validate the accuracy of the model.
- Model DRD motion and run simulations to gather the normal force data.
- Compare results of maximum normal force between all three types of drilling motion.
- Study power consumption at the drill bit and contact forces at the substrate particles to discuss the effect of drilling motion on penetration force.

2 Literature study

Chapter 2 will assess the state of recent literature with regard to both conventional and modern drilling methods and their mechanisms and governing laws, as well as numerical modeling techniques and research done in this field. Details on numerical techniques used to analyze the behaviors of granular materials, such as soil, are also introduced in this section. This literature review will highlight the knowledge gaps that this study intends to fill and provide perspective into the current state-of-the-art drilling technology as well as the theory needed to understand the process of drilling. Based on this, a research question and research goals will be formulated.

2.1 Conventional drilling

Rotary drilling emerged as a response to the challenges of accessing deeper and more remote oil and gas reserves during the Industrial Revolution. In the late 19th and early 20th centuries, traditional cable-tool drilling methods were reaching their limits, unable to penetrate the increasingly hard rock formations found at greater depths [20]. The breakthrough came with the realization that by employing rotational motion, rather than relying solely on percussive force, drilling efficiency could be vastly improved. Innovators like Howard Hughes Sr., Anthony F. Lucas, and others experimented with various designs, eventually perfecting the rotary drill rig. By attaching a rotating drill bit to the end of a drill string and circulating drilling fluid to remove cuttings and cool the bit, they unlocked the ability to drill faster, deeper, and more cost-effectively than ever before [33]. This technological leap laid the foundation for the modern petroleum industry, transforming the economics of resource extraction and fueling the rapid expansion of global energy production.

The mechanics of rotational drilling are governed by a complex interplay of forces and principles. As the drill bit delves into the Earth's crust, it applies a combination of downward force and torque, in accordance with Newton's laws of motion [42]. This dynamic interaction between the rotating bit and the geological formations relies on principles of friction and different material properties, dictating the efficiency and effectiveness of the drilling process. Meanwhile, the circulation of drilling fluid serves as a linchpin, embodying various principles of fluid mechanics and thermodynamics. Not only does the fluid cool and lubricate the drill bit, adhering to principles of heat transfer and fluid film lubrication, but it also serves as a medium for removing rock cuttings from the borehole, following Bernoulli's principle and the continuity equation [42]. Rotational drilling is celebrated for its versatility, effortlessly navigating diverse geological formations, from soft sediments to hard crystalline structures. This adaptability ensures efficient progress and optimal resource extraction, facilitated by high-speed rotation and continuous drilling fluid circulation, minimizing downtime [11]. However, alongside its strengths, rotational drilling faces significant challenges. Environmental impacts, including habitat disruption and noise pollution, require stringent regulations and sustainable practices. Additionally, operational complexity demands sophisticated equipment and expert personnel, with a focus on wellbore stability and formation evaluation. In formations with high abrasiveness or extreme hardness, drill bit wear and slow penetration rates can diminish efficiency, requiring frequent bit changes and increasing operational costs.

Percussive drilling is another popular drilling method that uses repeated impacts to break through hard rocks, commonly used in mining, geothermal, and construction applications. Its main benefits include faster penetration rates in hard rocks due to the very high thrust forces applied. However, it can be noisy, energy-intensive, and the vibrations may cause equipment wear or instability in certain conditions [33]. Percussive drilling is a preferred method to install offshore wind turbines because it efficiently penetrates dense and hard seabed materials, such as rock and compacted sand, by delivering repeated hammering impacts. This method provides better control in challenging underwater conditions, reduces the risk of tool jamming, and facilitates the deep installation of foundation piles. Additionally, it is faster and more cost-effective than other commercially available drilling methods. Unfortunately, the repeated high-impact forces have negative effects on the nearby sea life due to high noise levels and habitat disruption through seismic events. While previous research has highlighted the negative impacts on marine life around wind farms [14], there is little effort in changing the current practices with regard to wind turbine installation. This method is often applied in combination with rotary drilling, and a side-by-side example of a rotary drill and a drill using both rotation and percussion is shown in Figure 4 below.

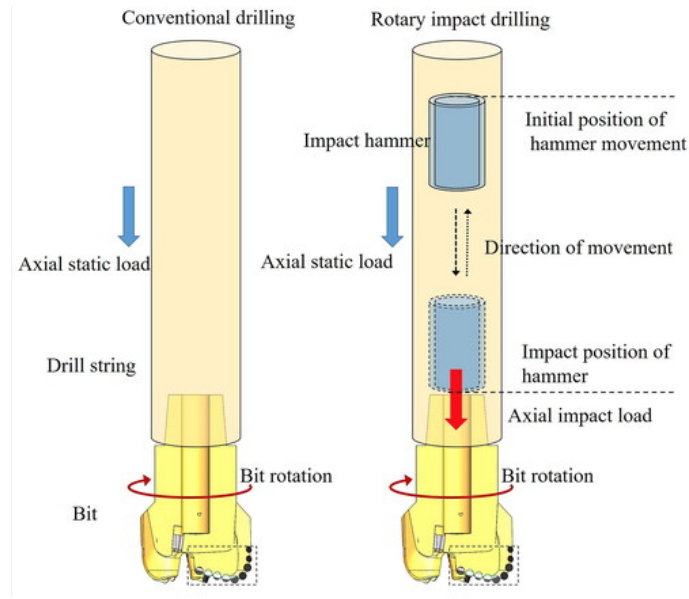


Figure 4: Example of industrial rotary and percussive drills [39]

In conclusion, while rotational drilling offers unmatched efficiencies in resource extraction, and percussive drilling excels in challenging environments, addressing environmental, technical, and financial challenges is essential. By embracing innovation and ecological stewardship, stakeholders can navigate these complexities and adapt to the evolving energy landscape with resilience and foresight.

2.2 Drilling and contact mechanics

Drilling is a complex process where precise control of forces is essential for both efficiency and accuracy. To analyze these forces it is important to understand what happens at the interface between the drill bit and the material being drilled. The interactions at this interface are critical, as they dictate how the material responds to the forces applied by the drill bit. These interactions govern material removal, heat generation, tool wear, and the overall stability of the operation. The forces at play here are not only responsible for the penetration of the material but also for how energy is transferred and dissipated at the contact surface. A deeper understanding of these forces is crucial for optimizing drilling performance, as even small damages at the interface can lead to tool failure, excessive wear, or poor surface finish, ultimately impacting the accuracy and productivity of the drilling operation. The prevalent forces that act on a drill bit during a drilling action are summarized below and shown in Figure 5.

- **Thrust** refers to the force exerted along the axis of the drill string. It is primarily responsible for advancing the drill bit into the formation. Thrust is crucial for breaking and removing rocks as the drill bit rotates and penetrates deeper into the subsurface.
- **Torque** is the rotational force applied to the drill string and ultimately to the drill bit. It is crucial for the cutting action of the bit as it rotates and penetrates the rock formation. It determines the rate at which the bit cuts through the formation and influences drilling efficiency. Insufficient torque may result in slow drilling progress, while excessive torque can lead to equipment damage or bit failure. Torque is influenced by several factors, including the rotary speed of the drill string, the diameter and design of the drill bit, the weight on the bit (WOB), and the mechanical properties of the formation being drilled.
- **Normal Force** is the perpendicular force exerted by the rock formation against the surface of the drill bit. This force is crucial in balancing the drilling operation, as it affects the bit's

stability and the interaction between the bit and the rock during penetration. This force is very important as it influences the contact between the bit and the formation, giving insight into the drilling operation itself, and is hence also known as the drilling force.

- **Friction Force** occurs between the drill bit and the rock formation as well as between the drill string components. It opposes the movement of the drill bit and affects drilling efficiency and energy consumption. Friction influences the rate of penetration, wear on the drill bit and drill string, and overall drilling performance. Proper lubrication, selection of drill bit materials, and optimization of drilling parameters help minimize frictional forces and improve drilling efficiency. The friction force is influenced by factors such as the surface roughness of the rock formation, the type and condition of the drill bit, the drilling fluid properties, and the weight on the bit (WOB). Adjustments to these parameters can help mitigate frictional effects and optimize drilling operations.
- **Shear** refers to the force applied parallel to the surface of the material being drilled, causing it to break or slide apart. As the drill bit cuts through the rock or formation, shear forces act at the bit's edges, helping to remove material by shearing it away from the formation.

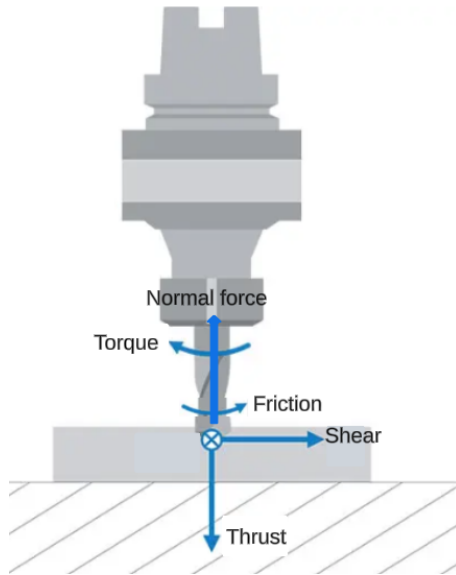


Figure 5: Example forces acting on a drill

While some of these forces are controlled directly by the drilling system's input, such as the thrust and torque, the other forces are direct results of intricate interactions between the drill bit and the soil and can be explained by contact mechanics. Contact mechanics is the study of how solid surfaces interact when they come into contact under applied loads. It focuses on understanding the distribution of stresses, deformations, and forces at the interface between contacting bodies. This field provides insights into how materials behave when they press, slide, or roll against each other, influencing phenomena like friction, wear, and material failure. There are many different methods to analyse contacts and this chapter aims to give a short introduction to the relevant models.

2.2.1 Material properties

To be able to understand the theory of contacts that will be introduced in this chapter, it is important to understand the parameters that influence it. Material properties describe the mechanical behavior of materials under different loads. Properties related to elasticity describe how materials deform and return to their original shape when subjected to stresses within their elastic limit. For small deformations, many materials exhibit a linear relationship between stress and strain, known as Hooke's law [12]:

$$\sigma = E \times \varepsilon \quad (1)$$

with E representing the modulus of elasticity of the material. Also known as Young's modulus, it measures a material's stiffness and is the ratio of tensile stress to tensile strain in the elastic region. It describes how much a material will stretch or compress under a given load, with higher values indicating stiffer materials [12].

Poisson's ratio (ν) relates the lateral contraction to the longitudinal extension when a material is stretched. It measures how much a material becomes thinner when stretched or thicker when compressed. A material with a Poisson's ratio of $\nu = 0.5$ is incompressible, meaning its volume does not change under pressure [30].

The shear modulus (G) is the ratio of shear stress to shear strain and describes the material's response to forces that cause one layer of the material to slide over another. It is related to the modulus of elasticity and Poisson's ratio by the equation [12]:

$$G = \frac{E}{2(1 + \nu)} \quad (2)$$

When looking at a material as a whole, and not only at what is happening at its surface, it is also important to consider its bulk modulus K . It measures how resistant a material is to uniform compression and it is given as a function of the Poisson's ratio and Young's modulus [30]:

$$K = \frac{E}{3(1 - 2\nu)} \quad (3)$$

2.2.2 Normal contacts and Hertzian contact theory

To begin the understanding of contact mechanics, it is important to first look at normal forces between two bodies that are brought into contact with one another. Normal contact without adhesion refers to the interaction between two solid bodies that come into contact under an applied load, with no attraction between the surfaces. In this type of contact, the bodies deform elastically or plastically depending on the material properties, but there is no additional force pulling the surfaces together beyond the externally applied load [30]. The classic example is Hertzian contact, which models how two elastic bodies, like spheres or cylinders, behave when pressed together. In this scenario, the contact area grows with increasing load, and the stresses are distributed across this area according to the material stiffness and geometry. The absence of adhesion simplifies the analysis by focusing solely on the deformation caused by the normal forces, making it highly relevant for applications like bearings, gears, and rolling contacts where the primary concern is the load-bearing capacity rather than adhesive effects.

Hertzian contact theory describes the behavior of two elastic bodies in contact under a normal load, focusing on the stresses, deformations, and contact area formed at the interface. Developed by Heinrich Hertz in 1881, the theory assumes no adhesion or friction between the surfaces, and that the materials are homogeneous and elastic [30]. Here, the penetration depth is related to the contact radius through the relationship:

$$a^2 = Rd \quad (4)$$

where d is the penetration depth, a is the contact radius and R is the equivalent radius which depends on the radii of the contacting spheres through the following relation:

$$\frac{1}{R} = \frac{1}{R_1} + \frac{1}{R_2} \quad (5)$$

The total normal force is given by:

$$F_n = \frac{4}{3}E^*R^{1/2}d^{3/2} \quad (6)$$

E^* represents the reduced elastic modulus which accounts for the elastic properties of two different materials in contact. It simplifies the interaction by combining the elastic moduli and Poisson's

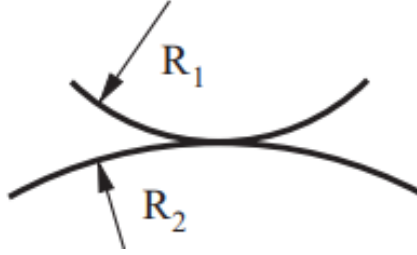


Figure 6: Sphere to sphere contact [30]

ratios of both materials into a single value, which can be used in calculations for contact stress and deformation [30]. If both bodies in contact are elastic, then the following expression is used:

$$\frac{1}{E^*} = \frac{1 - \nu_1^2}{E_1} + \frac{1 - \nu_2^2}{E_2} \quad (7)$$

Hertzian contact theory aims to describe:

- a.) The relationship between the contact force and the normal displacement of the body.
- b.) The relationships between normal contact force and contact stresses.

However, with sliding contacts, there will still be relative motion in the tangential direction, because of the differences in the transverse contraction of the bodies in contact, making tangential and frictional forces in the surface layers come into play [30].

When a drill bit makes contact with soil, the interaction can be modeled as a normal contact, more specifically a Hertzian sphere-to-sphere contact, as the soil particles can be represented by a granular bed of perfect spheres (Figure 6).

2.2.3 Friction in sliding contacts

With the increasing complexity of the understanding of contact mechanics, it is important to consider the effects of frictional forces on the systems in contact. Friction between solid bodies is an extremely complex phenomenon that encompasses elastic and plastic deformations of contacting surfaces, wear particle interactions, micro-fractures, energy, and many other factors. The simplest explanation of friction can be given through Coulomb's law of dry friction, which states that frictional force is proportional to the normal force and independent of the speed, contact area, and roughness. It is a first-order approximation and uses the notion of a coefficient of friction as a rough, first approximation of the quotient of frictional force to normal force [30]. The Coulomb's friction law is shown in Equation 8 below.

$$F_{fr} = \mu F_n \quad (8)$$

The coefficient of static friction can be determined experimentally by measuring the inclination angle at which a body lying on an inclined plane begins to slide. This angle is known as the angle of friction, and it is represented by the symbol φ in Figure 7. At the angle of friction, the static force reaches its limit and the equilibrium of forces in this critical state is used to derive the relation between the angle of friction φ and the coefficient of friction μ , shown in Equation 9.

$$\tan \varphi = \mu_s \quad (9)$$

Friction can be separated into static and kinetic friction. Static friction is the critical force that needs to be overcome to put a resting body in motion. Kinetic friction is the resisting force that acts on a body after the force of static friction has been overcome. Both of these forces follow the law in Equation 8, and their respective coefficients of friction are approximately equal ($\mu_s = \mu_k$).

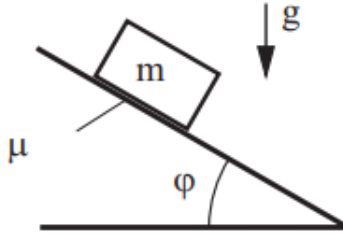


Figure 7: A body on an inclined plane [30]

However, this linear dependence of the frictional force on the normal force is only applicable to a specific force domain (not too small and not too large). This dependence is no longer valid if the real contact area is comparable to the apparent contact area [30]. Softer materials and polymers can very easily reach this limit. Additional considerations need to be made when reviewing the sliding speed. For simplicity it is assumed that the coefficient of kinetic friction does not depend on sliding speed. This approximation is invalid for very low and very high speeds.

The Mindlin-Deresiewicz contact theory builds on classical Hertzian contact mechanics to describe the behavior of two elastic bodies under combined normal and tangential loads, including the development of frictional forces at the contact interface. This theory is essential for understanding the transition from static friction to sliding (kinetic) friction.

According to Mindlin-Deresiewicz, when a tangential force is applied between two bodies in contact, their response depends on whether the surfaces slip or remain in a no-slip condition. Initially, the contact remains in a partial slip condition, where a small zone near the contact edge begins to slip while the rest of the contact area remains stuck. As the tangential force increases, the slip zone grows. The tangential stiffness of the contact resists the applied force until the limit defined by static friction is reached. At this point, full sliding occurs, and the bodies transition from static to kinetic friction [32].

This is not discussed further as, in the case of working with Discrete Element Method (DEM) simulations, for simplicity, the tangential forces are typically analyzed under the assumption of a no-slip condition, and a rather approximated model of Mindlin-Deresiewicz theory is applied. This simplification is used because it allows easier modeling of the tangential interactions without needing to account for the complexities of partial slip and sliding behavior. In the no-slip condition, the applied tangential forces do not cause relative motion between the two contact surfaces. Instead, the force is entirely absorbed through elastic deformation in the contact area. The elastic deformation generates shear stresses and small displacements in the material, but the surfaces remain "stuck" due to the static friction between them. The no-slip condition holds as long as the tangential force does not exceed the maximum static friction, which is proportional to the normal force exerted between the bodies and the coefficient of static friction [29]. In this study, the term Mindlin's contact theory is therefore used loosely, as it refers to only the DEM approximation of this theory, which encompasses much less than the theory's original grasp. To be exact, DEM replaces Mindlin's laws with a simplified linear correlation by using a simple linear spring model.

$$F_{\text{tangential}} \leq \mu_s F_{\text{normal}} \quad (10)$$

The DEM theory is introduced in Chapters 2.5 and 2.6.

2.2.4 Theory of adhesive contacts

While the normal contact theory, only takes into account the geometrical, physical contact of bodies, in reality, there exists a relatively weak force between any two bodies, which dissipates with larger distances between objects. These forces lead to mutual attraction between bodies and are known as adhesion forces. Adhesive contact in a tribological context refers to quasi-instantaneous adhesion between contacting surfaces as a result of van der Waals forces or electron transfer. These forces play a major role in contacts that include one soft object or when the system is being analyzed on a microscopic level.

The first simplified adhesion models appeared in 1932 with R.S. Bradley defining the adhesive force between a rigid sphere and a rigid plane. The interaction energy is calculated between two bodies using the Half-Space approximation, such that the contact area is assumed to be significantly smaller than the radius of the sphere, which allows for the surfaces to be viewed as parallel [30].

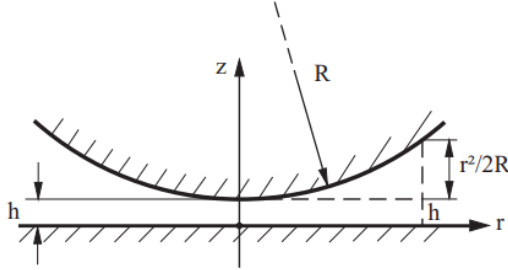


Figure 8: Rigid cone penetrating elastic half-space [30]

The adhesive force was calculated using the equation:

$$F_{adh} = -\frac{2\pi RQ}{r_0^2} = -4\pi\Delta\gamma R \quad (11)$$

where Q is the potential energy, r_0 is the equilibrium distance and $\Delta\gamma$ is the inetraction energy [30].

While the Bradley model is valid for completely rigid bodies, it was only in 1971 that Johnson, Kendall, and Roberts presented the solution for adhesive contacts between elastic bodies, in what is now known as the JKR-Theory [30]. They determined that the adhesive force is described by the following relation:

$$F_{adh} = -\frac{3}{2}\Delta\gamma\pi R \quad (12)$$

The JKR model of adhesion is used further in this study to analyze adhesive contacts.

2.2.5 Capillarity

Capillary forces in contact mechanics arise due to the interaction between liquid films and solid surfaces, particularly at small scales. These forces are driven by *capillarity*, which is the ability of a liquid to flow in narrow spaces without the assistance of external forces (such as gravity). This occurs due to the combination of *surface tension* and *adhesion* between the liquid and solid surfaces [30]. In contact mechanics, capillary forces become significant when a liquid bridges the gap between two solid surfaces. These forces can either enhance adhesion or lubricate contact depending on the system.

Capillarity is a specific form of adhesion that involves the presence of a liquid between surfaces. Adhesion in general refers to the attractive forces between two surfaces, which can be mediated by van der Waals forces, electrostatic forces, or liquid bridges. Capillary adhesion, on the other hand, occurs when the liquid bridge pulls the surfaces together through the action of surface tension.

In the context of soil drilling, capillary forces play a critical role, particularly in unsaturated soils. These forces arise from the presence of water films around soil particles, influencing the soil's strength, cohesiveness, and resistance to penetration. The capillary forces contribute to the *suction pressure* in the pores, which can either increase the difficulty of drilling (by increasing the effective stress) or make soil collapse easier when the liquid bridges break down. Understanding these forces is crucial in predicting soil behavior during drilling and excavation, especially when dealing with partially saturated soils [8].

The theoretical background of capillarity is based on the *Young-Laplace equation*, which relates the pressure difference across a liquid interface to surface tension and curvature. Capillary forces

are computed by considering the geometry of the liquid bridge between two surfaces, the surface tension of the liquid, and the contact angle (governed by the liquid's wetting properties) [8]. One common equation for the capillary force is:

$$F_{\text{cap}} = -2\pi\gamma R \cos(\theta) \quad (13)$$

This formula represents the capillary force acting between a spherical surface and a flat surface (or between two spheres), where γ is the *surface tension*, R is the *radius of the contact area*, and θ is the *contact angle*. The negative sign indicates that the force is attractive, pulling the surfaces together. This expression simplifies the capillary force by focusing on the surface tension of the liquid bridge and its wetting properties [8]. It is typically used in *Hertz-like* or *DMT-like models*, where capillary adhesion dominates the interaction.

In the context of adhesion, an important concept is the *work of adhesion*, which quantifies the energy required to separate two surfaces from contact. When a liquid bridge is present, the capillary forces increase the work of adhesion, making it harder to separate the surfaces. This is particularly important when surface tension (the cohesive forces within the liquid) and adhesion between the liquid and the solid surfaces interact to generate capillary adhesion.

2.3 Biomimicry in drilling

Biomimicry is an approach that seeks to solve human challenges by emulating nature's designs and processes. By studying the strategies and structures in organisms, scientists and engineers can create more efficient, sustainable solutions. This practice leverages nature's time-tested solutions to address complex problems in fields ranging from technology to medicine. Biomimicry not only inspires new designs but also fosters a deeper understanding of ecological systems and their interconnectedness. It encourages the development of technologies that harmonize with natural processes, leading to sustainable innovations that minimize environmental impact and enhance the resilience of both human and natural systems. By drawing on the wisdom of nature, biomimicry helps bridge the gap between human ingenuity and ecological balance, while finding effective and rapid solutions to complex issues.

2.3.1 Drilling in the animal kingdom

There are many examples of organisms using different drilling strategies in their everyday lives. For example, the sand snake's remarkable ability to glide through the sand with minimal resistance is due to its unique, wave-like motion, also known as undular motion. This serpentine movement reduces friction and allows the snake to navigate through granular materials effortlessly. Similarly, earthworms create channels in the soil by contracting and expanding their bodies, which allows them to move through and aerate the earth efficiently. This natural strategy highlights the potential for designing drilling systems that can adapt to varying soil conditions and self-clean or maintain their functionality in challenging environments. The worms' ability to process soil and create stable tunnels demonstrates how leveraging natural processes can lead to advancements in drilling technology that are both effective and adaptable. Another compelling example comes from the octopus, known for its suction-based drilling capabilities. Octopuses use their specialized suckers to grip and manipulate surfaces, including creating powerful suction to drill into substrates. All of these animals had millions of years of evolution to perfect the way in which they use their bodies for drilling purposes, leaving a lot to learn from their examples. Since living organisms use their extremities, or their whole bodies to perform drilling actions, the way in which they reduce what we would call "tool wear" becomes paramount.

2.3.2 The wood wasp drilling mechanism

As mentioned in Chapter 1, the wood wasp has developed a specialized organ called an ovipositor that is responsible for drilling wood bark and depositing the wasp's eggs. The ovipositor of the wood wasp operates through a process known as dual reciprocation drilling (DRD). This mechanism involves two distinct but coordinated movements that enable the wasp to penetrate the wood efficiently. The ovipositor typically comprises two lower or ventral valves and one upper or dorsal valve. The basic drilling process involves a dual reciprocation mechanism where the valves move

back and forth in a coordinated fashion. When one valve extends outward, the other retracts, and vice versa. This reciprocating motion is crucial for effective drilling [2]. The valves are equipped with teeth that engage with the wood surface. In species like *Sirex noctilio* and *Megarhyssa nortoni*, these teeth are arranged differently, influencing their drilling effectiveness. For example, the teeth at the tip of the ovipositor in *M. nortoni* point proximally, which aids in breaking the wood cell walls in tension. Conversely, *S. noctilio* has teeth that alternate in orientation, affecting how the ovipositor interacts with the wood. During the drilling process, the initial forward stroke of the ovipositor's teeth penetrates the wood, creating a groove. This groove allows the subsequent strokes to drive deeper into the wood [13]. The movement of the valves involves significant forces. The downward stroke of the ovipositor must push through the wood's cell wall, which requires considerable force. This force is initially limited by the buckling strength of the ovipositor, but it is enhanced by the tensile forces generated as the proximal teeth engage with the wood and pull against it. Essentially, the upward motion of the ovipositor's teeth exerts a pulling force that helps to break the wood's cell walls, while the downward motion is supported by the structural integrity of the ovipositor [13]. In the case of *M. nortoni*, studies have shown that the tension force exerted by the proximal teeth can be up to ten times higher than the critical buckling load of the ovipositor [19]. This means that the force applied during the downward stroke is predominantly a result of the resistance provided by the wood against the upward-moving, tensioned part of the ovipositor. This dual mechanism allows the wood wasp to effectively penetrate and drill into wood, demonstrating an impressive example of evolutionary adaptation for oviposition in challenging environments. It remains a possibility that these specialized drilling techniques could be applied to industrial drilling exploits, however, the feasibility of this needs to be studied further. The schematic representation of this process is given in Figure 9 below.

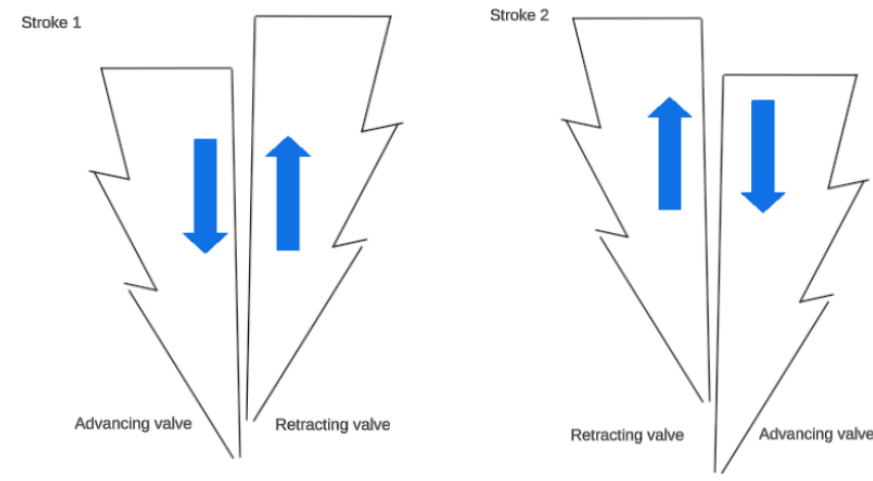


Figure 9: Schematic of dual reciprocating drilling principle used by wood wasps [13]

2.3.3 Numerical and experimental advances in DRD research

Despite the proposed evolutionary importance of the ovipositor, empirical studies on its mechanical properties are limited. Understanding the ovipositor's probing and steering mechanisms can provide insights into the evolutionary success of the wood wasp and aid the development of minimally invasive drilling tools. Through automated image processing and custom tracking algorithms, the research of Crkvenik [37], successfully extracted 3D trajectories and valve kinematics of the ovipositor in *Diachasmimorpha longicaudata*, another species of wood wasps, allowing for the precise quantification of insertion speeds, valve protraction, and curvature during probing. The results indicated a clear relationship between substrate density and the speed of insertion, with higher densities leading to slower speeds. These detailed measurements revealed the remarkable efficiency of wasp ovipositors in penetrating soft, variable-density materials. By employing a reciprocating motion, the wasps were able to minimize the force applied during insertion, demonstrating an elegant adaptation to their environment.

Another wealth of knowledge regarding dual reciprocation comes from the research of Mohamed Alkalla, which mostly investigated the effects of varying drill bit geometries and substrates [2]. He concluded that different drill bit designs perform uniquely depending on the material drilled. The concave drill profiles excelled in soft regolith due to better penetration, while the convex profiles with helical teeth are more effective in harder formations, aiding in traction and cutting removal. In fine-grain regolith, helical teeth are less efficient as they tend to carry particles instead of removing them. Rhombic cross-section bits reduce drilling time by minimizing the exposed area under pressure. The study suggests customizing drill bits for different surfaces, with convex and concave profiles suited for hard or icy regolith. In his paper on the development of a Dual-Reciprocating Oscillation Drill (DROD) for extraterrestrial drilling and sampling, further research was done on the effects of drill bit geometry in dual reciprocating drilling [3]. Through simulations, the study revealed that particle friction and interlocking impact the effectiveness of toothed drill bits during reciprocation, while tool-surface friction is critical for toothless bits. He also concluded that the performance of the drill was greatly dependent on whether the drilling motion was able to fluidize the regolith.

While important, the numerical research done so far has greatly focused on understanding and optimizing the reciprocating motion and parameters such as the drill bit geometry, and not on comparing its performance to current conventional methods. The main focus on the application of such drills was on small-scale extraterrestrial expeditions and not on any industrial-size operations that are currently happening on Earth.

There is also a limited amount of experimental testing done on dual reciprocating drilling. Studies conducted at InTech [26] aimed to analyze different ways in which reciprocation can be applied to drilling and to determine the most important parameters that influence this type of drilling. This study identified three main factor groups that will determine the success of reciprocating drilling: drill head geometry, substrate parameters, and operational parameters. The laboratory setup used in these studies closely resembled the one at the University of Twente shown in Figure 3b, however, there are a few key differences. Mainly, this setup is equipped with a data acquisition system and multiple sensors, as well as a control chain. The motor used by this machine is a continuous current motor and the reciprocation amplitude of the drill bit can be varied.

The most important DRD parameters defined in this study are the substrate density and consistency, frequency of reciprocation, and amplitude or stroke length of reciprocation. It is clear that the current DRD setups are in their early stages, and that more work needs to be done to optimize the system for any industrial use. While research into reciprocating drilling has been on the rise in the last few years, there were no studies done to directly compare the efficacy of traditional drilling methods to DRD in these sectors. To aid the transition to sustainable practices, it is necessary to investigate whether dual-reciprocating drilling can provide the same or better performance than the current drills on the market while consuming less energy and causing less harmful effects on the environment.

2.4 Use of simulations in drilling

As experiments can be time-consuming and expensive, the development of numerical models to simulate the behavior of bodies or particles has greatly affected the development time of new technologies. Conventional methods like the Finite Element Method (FEM) often struggle with accurately modeling large-scale deformations and discontinuities, such as cracks and granular mechanics. To overcome these limitations, newer methods like the Discrete Element Method (DEM) and Bonded Particle Method (BPM) have been introduced. These methods focus on simulating interactions between discrete particles, offering a more effective way to model large-scale granular shear and deformation [4]. As a result, DEM and BPM have become crucial tools across various engineering disciplines, especially for analyzing materials with brittle behavior, and continue to be refined to accommodate an even broader range of applications. The Discrete Element Method (DEM) is recognized as a valuable tool for studying the deformation behavior of regolith and its interactions with tools. It models macroscopic regolith behavior by analyzing particle interactions at the microscopic scale. DEM has been applied to various aspects of regolith research, including excavations, sampling, wheel interactions, and drilling, though challenges remain in accurately replicating experimental forces due to limitations like particle shape and number [28]. The Bonded Particle Method (BPM) enhances the Discrete Element Method (DEM) by introducing an ad-

ditional algorithm that enables the simulation of continuum mechanics, making it essential for geomechanical analyses where material cohesion is significant, such as in rocks and soils. BPM models the interaction between grains and the cement that binds them, reflecting real geological formations like sandstone. While pure DEM is suitable for cohesionless materials, BPM is necessary for capturing the resistance to external forces in cohesive materials. BPM allows for the simulation of complex behaviors, including fracture, elasticity, and post-peak softening, by modeling grain-to-grain interactions and the gradual transition from a bonded state (BPM) to a granular state (DEM). This method is widely used in various software platforms, offering flexibility in simulating the mechanical behavior of materials with both bonded and unbonded particles [4]. In this case, open-source DEM solver YADE is used, but there are many options to choose from.

While DEM and YADE will be described in more detail in the next section, it is worth looking into the current advancements in drilling simulations. Numerical modeling of DRD drilling, while scarce, has greatly focused on optimizing frictional losses in the actuation setup and optimizing the drill bit interface for drag minimization [28]. Great insight into DRD modeling comes from the research of Alkalla et al. [3] who performed a kinematic and dynamic analysis using MATLAB and coupled it with a DEM platform called Edem. This research focused on extraterrestrial drilling and how different drill bit geometries influence DRD. Another great insight into the process of numerical modeling comes from A. Amiri [4], who validated his numerical model on simple penetration testing before moving on to modeling complex drilling interactions. However, none of this research directly compares DRD to different types of drilling motions. While arguments like regolith fluidization due to oscillation and high overhead force generation support the benefits of DRD, a more comprehensive study to determine its benefits is needed. This study aims to offer a comprehensive DEM analysis of DRD. Using DEM for simulating dual reciprocating motion offers several advantages over traditional continuum-based approaches. DEM is particularly effective in modeling granular or particulate materials, which makes it ideal for studying interactions in complex, heterogeneous substrates. Unlike finite element methods, DEM captures individual particle behavior and their interactions, allowing for more accurate simulation of dynamic forces, deformations, and penetrations during reciprocating motion. This approach enables a detailed analysis of how dual reciprocating systems can potentially reduce applied forces and improve efficiency in material penetration.

2.5 Discrete Element Method - DEM

Discrete Element Method (DEM) is a numerical technique employed in engineering and physics applications to simulate the behavior of systems comprising discrete, interacting particles. Unlike traditional continuum-based methods, DEM focuses on modeling individual particles and their interactions, making it particularly suited for the analysis of granular materials, powders, and particulate systems [36]. In DEM simulations, each particle is represented as an individual entity with specific attributes such as mass, shape, and surface properties. The interactions between these particles are defined by contact models, incorporating forces, torques, and constraints that govern their motion. The simulation progresses in discrete time steps, allowing for the accurate tracking of particle movements and dynamic changes in the system. Figure 10 shows an example DEM simulation done on a rotating drill bit.

2.5.1 Working principles

The Discrete Element Method (DEM) functions by simulating the behavior of a system of discrete particles, tracking their interactions and movements over time. Initially, particles are generated with specific properties such as size, shape, mass, and material characteristics, and their initial positions and velocities are defined. The simulation domain is established with appropriate boundary conditions. Each simulation cycle begins with detecting which particles are in contact using spatial search algorithms [40]. One common approach is the Verlet list [23], which involves creating a list of potential neighbors for each particle within a certain cutoff distance. This list is periodically updated as particles move, ensuring that only nearby particles are considered for contact calculations, significantly reducing computational effort. For contact detection during this study, a Linked Cell

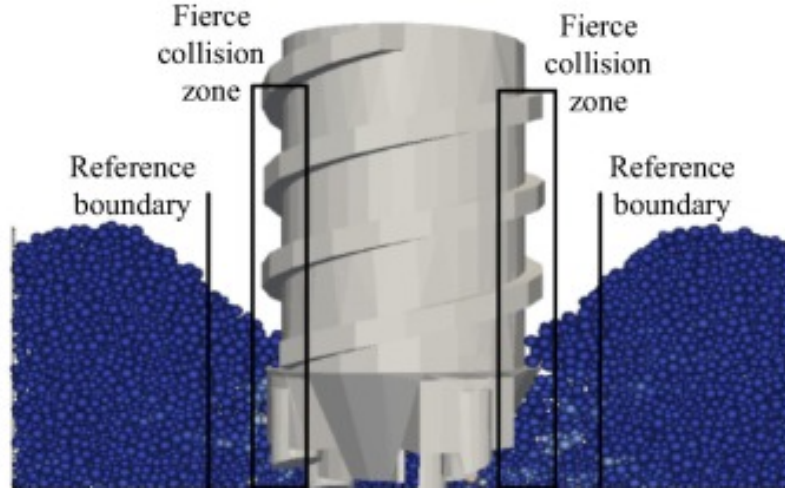


Figure 10: Example DEM model of a rotating drill bit [24]

method is used [23]. This method divides the simulation domain into a grid of cells, with each cell tracking the particles within it. Particles are assigned to cells based on their coordinates, and the algorithm searches for potential contacts within the particle's cell and neighboring cells, significantly reducing the number of distance calculations. This localized search updates at each time step as particles move, ensuring efficient and accurate contact detection. The Linked Cell method's efficiency and scalability make it ideal for large-scale simulations, maintaining computational feasibility while handling complex particle interactions. Normal forces between particles are then calculated based on their overlap, often using Hertzian contact theory, while tangential forces are determined through models like the Coulomb friction law. Damping forces are included to simulate energy dissipation. The equations of motion are then integrated over time to update the velocities and positions of the particles, using methods such as the Verlet integration for computational efficiency. This process repeats for each time step until the simulation concludes, with data recorded for analysis. The summarized Linked Cell algorithm used by YADE is depicted in Figure 11 below.

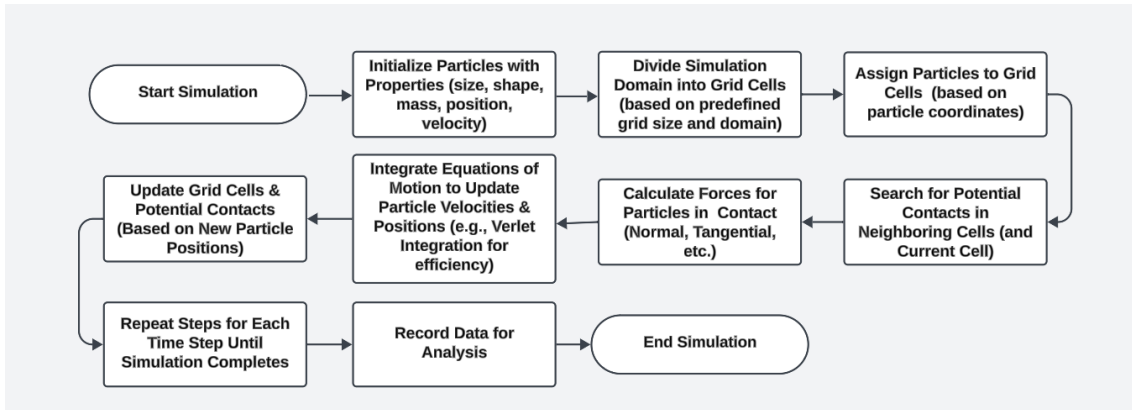


Figure 11: Linked Cell algorithm in YADE [40]

The governing principles of the Discrete Element Method (DEM) revolve around contact mechanics, which describe how particles interact when they come into contact. When two particles come into contact, several forces are at play, and understanding these forces is crucial for accurately modeling their behavior. Normal forces are the forces acting perpendicular to the surfaces of the particles at the point of contact. In DEM, these forces can be calculated based on the Hertzian contact theory described in Chapter 2.2.2 or by a simplified linear-elastic model (Cundall-Strack) shown in equation 14. These computations get updated incrementally, with each time step.

$$\Delta F_n = K_{normal} \Delta u_n \quad (14)$$

Here ΔF_n is the normal force, Δu_n is the overlap or penetration between the two contacting particles in the normal direction, and K_{normal} is the normal stiffness at the contact, which can be calculated using equation, or taken as a constant for a given material and geometry if Cundall-Strack model is used.

$$K_{normal} = \frac{2}{3}E^*\sqrt{R'\delta} \quad (15)$$

As previously mentioned, the Mindlin-Deresiewicz theory in DEM is approximated by a linear model to extend the Hertzian contact theory and account for tangential forces and frictional effects. Tangential forces arise due to relative tangential motion (e.g., sliding or rolling) between particles at the contact point. For simplicity, Mindlin's theory is only approximated in DEM and the no-slip condition is applied to analyzing tangential forces. The maximum tangential force is constrained by Coulomb's friction law in equation 10, which dictates that the tangential force is limited by the product of the normal force and the coefficient of friction, beyond which slip occurs. Tangential forces before the slipping of the contact are calculated incrementally, based on a simplified linear spring model, following equation 16.

$$\Delta F_s = K_{shear}\Delta u_s \quad (16)$$

Here, Δu_s is the incremental shear displacement, ΔF_s is the incremental shear force and K_{shear} is the shear stiffness at the contact point, which is usually taken as a constant value. If the Hertz-Mindlin model is used, this value is taken proportional to the normal stiffness divided by a dimensionless factor [40].

For materials with cohesive or adhesive properties, additional forces need to be included in the simulation. Cohesion refers to the attractive force between particles of the same material, while adhesion refers to the attractive force between different materials. Models such as the JKR (Johnson-Kendall-Roberts) theory [5] can be used to describe these forces as discussed in Chapter 2.2.4. Capillary forces are difficult to model using DEM since capillary bridges may form between the particles that are not in direct contact with each other. This is why capillary forces are not standardized in DEM but have to be modeled based on empirical data on a case-to-case basis. These concepts will be discussed more in Chapter 4.4.2.

In real-world systems, energy is dissipated through various mechanisms such as internal friction, plastic deformation, and other dissipative processes. DEM simulations include damping terms to account for these energy losses. Damping can be linear or non-linear and affects both normal and tangential components of the contact forces. The damping coefficient can be defined for all DEM simulations to fit the needs of specific applications.

Finally, time integration techniques ensure that the equations of motion are integrated over time to update the velocities and positions of the particles. Common time integration methods include:

- **Explicit methods:** These methods, such as the Verlet integration or Leapfrog method, update the positions and velocities directly based on the current accelerations. They are simple and computationally efficient but require small time steps for stability [36].
- **Implicit methods:** These methods, such as the Newmark-beta method, are more stable and can handle larger time steps but are computationally more intensive, which is why in this study the first method is used [36].

2.6 YADE software

YADE, which stands for "Yet Another Dynamic Engine," is an open-source Discrete Element Method (DEM) software package specifically designed for simulating the behavior of granular materials and interacting particles. Developed in Python with a C++ core, YADE provides a flexible and extensible platform for researchers and engineers to conduct simulations of complex particulate systems. The software's open-source nature allows users to customize simulations, implement new contact models, and integrate additional features to suit specific research needs. YADE's capabilities make it particularly valuable for investigating drilling processes, providing a platform to simulate the intricate interactions between drill bits and subsurface materials in a granular context.

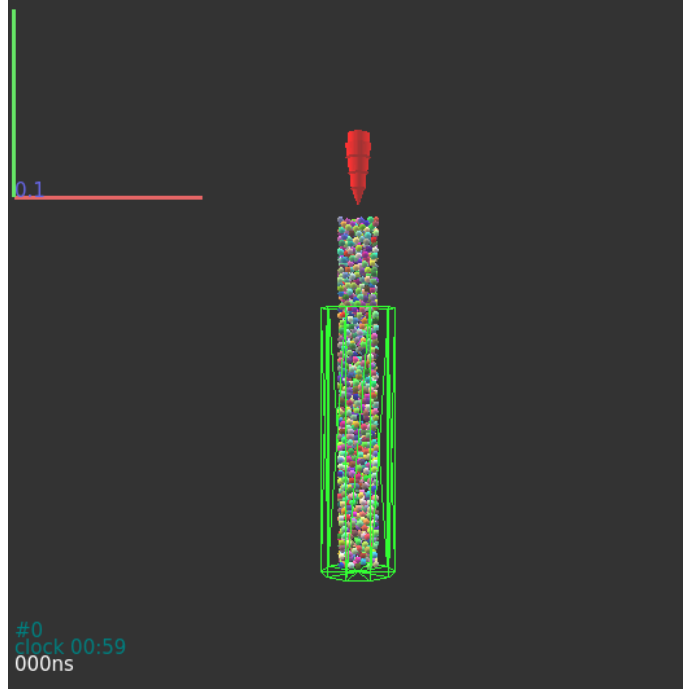


Figure 12: Simulation of drilling in YADE software

In YADE, the contact laws define the interactions between individual particles, determining the forces, torques, and constraints governing their motion. YADE offers a range of contact laws that users can choose based on the specific characteristics of the simulated material. Some common contact laws implemented in YADE include linear spring-dashpot, linear Hertz-Mindlin, linear isotropic elastic, and the rolling friction model [40]. These contact laws allow users to capture a wide range of particle interactions, accounting for factors such as particle shape and material properties. They are discussed further in the following sections. In YADE, the basic DEM principles and calculations introduced in the previous section are applied. Furthermore, YADE allows for the tracking of other relevant physical quantities, such as velocities, accelerations, and particle rotations, providing a detailed understanding of the dynamic behavior of the simulated system.

2.6.1 Contact laws

Contact laws are mathematical models that describe the interactions between particles in a discrete element method (DEM) simulation. YADE, an open-source DEM software, employs these contact laws to simulate the mechanical behavior of granular materials under various conditions. The choice of contact law significantly affects the accuracy and realism of the simulation results.

One of the more sophisticated contact laws in YADE is `Law2_ScGeom_MindlinPhys_Mindlin()`. In YADE, this law replaces Mindlin’s contact theory with a linear model that accounts for both normal and tangential forces that develop when particles come into contact [36]. The normal force is computed using Hertzian contact theory, which relates the force to the elastic deformation of the particles. The tangential force calculation is more complex, considering the history of tangential displacement and incremental shear forces, which makes it capable of capturing the detailed frictional behavior and elastic hysteresis of the materials. The history of particle interactions is primarily tracked through the cumulative tangential displacement and incremental shear force calculations [36]. Tangential force calculations are based on equation 16 introduced in the previous section. This law is particularly valuable for simulating more realistic behaviors in granular materials, such as soil or powders, where the history of particle interactions significantly influences the material response.

In contrast, the Cundall-Strack contact law (`Law2_ScGeom_FrictPhys_CundallStrack()`) is a simpler model. It uses a linear-spring system to represent both normal and tangential interactions. The forces are directly proportional to the displacements, with linear stiffness and damping

coefficients [36]. The Hertz-Mindlin model from before only simplified the tangential interactions. While this approach is computationally efficient and easier to implement, it lacks the detailed physical realism of the Mindlin model. It does not account for the complex history-dependent behavior of tangential forces, making it less suitable for scenarios where an accurate representation of material behavior under cyclic loading or complex interactions is crucial.

Despite the computational simplicity of the Cundall-Strack model, the Mindlin contact law is generally more appropriate for accurately simulating experiments, even those involving rigid contacts. By setting very high elastic moduli in the Mindlin model, one can approximate rigid behavior while still capturing the essential physics of particle interactions. This approach, although more computationally demanding, provides a more realistic simulation of material behavior compared to the linear assumptions of the Cundall-Strack law. Thus, in the course of this study, the Hertz-Mindlin model is used.

2.6.2 Engines

In YADE, engines are fundamental components that define the sequence of operations in a simulation. They dictate how the simulation progresses over time, controlling aspects such as force calculations, collision detection, and particle movements. By combining different engines, users can customize the simulation process to accurately model the physical behavior of granular materials and other discrete systems. Engines are executed in a loop, with each iteration representing a small time step in the simulation. A summary of the algorithm for the O.engines function in YADE is laid out in Figure 13 [40].

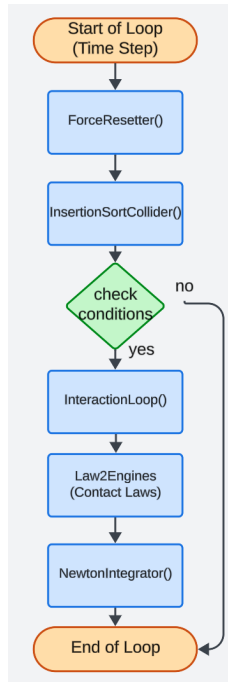


Figure 13: YADE engine loop execution

The **ForceResetter()** engine, for instance, resets the forces on all bodies at the beginning of each iteration, ensuring that only the current forces are considered. The **InsertionSortCollider()** engine detects potential collisions between bodies by sorting them based on their spatial coordinates, which is computationally efficient for large systems. It utilizes `Bo1_Sphere_Aabb()` and `Bo1_Facet_Aabb()` to handle the bounding boxes of spheres and facets, respectively, enabling accurate collision detection [40].

The **InteractionLoop()** engine is the core of the contact force computation, involving three components: interaction geometry (`Ig2_*`), interaction physics (`Ip2_*`), and the contact law (`Law2_*`). Here `Ig2_Sphere_Sphere_ScGeom()` and `Ig2_Facet_Sphere_ScGeom()` determine the geometric

relationships between colliding bodies, while `Ip2_FrictMat_FrictMat_MindlinPhys()` computes the physical properties of the contacts. The contact forces are then calculated using `Law2_ScGeom_MindlinPhys_Mindlin()`, which models both normal and tangential forces with high accuracy [40].

The **NewtonIntegrator()** engine is responsible for updating the positions and velocities of bodies based on the computed forces and torques, incorporating gravitational effects and damping to simulate energy dissipation [40].

Additionally, the **TranslationEngine()** is used to apply a constant translation to specific bodies, such as moving a set of particles or a rigid object along a defined axis at a specified velocity. In this case, it translates bodies along the negative y-axis at a velocity of 0.01 m/s. This engine is labeled as 'translation' and can be activated or deactivated as needed [40].

Another useful engine is the **RotationEngine()**. This engine applies a rotational motion to specified bodies, allowing for the simulation of rotating machinery or the imposition of angular velocities on particles. By specifying the rotation axis and angular velocity, the `RotationEngine()` can induce realistic rotational behavior, which is crucial for modeling systems where rotation plays a significant role, such as in mixers or rotating drums [40].

Overall, YADE engines provide a versatile and powerful framework for simulating complex physical systems. By carefully selecting and configuring these engines, users can achieve highly accurate and realistic simulations tailored to their specific experimental or research needs.

2.6.3 Particle representation

Particles in YADE are typically represented as spheres, although the software also supports other shapes such as boxes and facets. The choice of particle shape depends on the specific application and the level of detail required. For instance, spheres are commonly used due to their simplicity and the ease with which they model isotropic interactions, while facets or polyhedra can be used for more complex shapes that better approximate real-world objects. Each particle is defined by its geometric properties, such as radius, position, and orientation, as well as its physical attributes, including density, elasticity, and frictional properties.

2.6.4 Contact detection and resolution

In YADE, contact detection and resolution are pivotal processes that ensure accurate simulations of particle interactions. Contact detection starts with identifying when and where particles come into contact, utilizing spatial partitioning techniques such as bounding volume hierarchies or cell-based methods [6]. The `InsertionSortCollider` engine is a key component in this process, sorting particles into spatial bins to efficiently manage collision checks. By focusing computational resources on particle pairs that are close enough to interact, YADE optimizes the process and reduces unnecessary calculations. Geometric algorithms then determine the exact contact points and overlaps between particles. For spherical particles, this involves comparing the distance between their centers with the sum of their radii. For more complex shapes, such as facets or polyhedra, YADE employs advanced algorithms to assess intersections and contact areas. The main collision detection algorithm in YADE is the Sweep and Prune algorithm which optimizes the detection of potential collisions by sorting axis-aligned bounding boxes (AABBs) along each axis (x, y, z). It works by maintaining sorted lists of the minimum and maximum coordinates of AABBs for each axis. By identifying overlaps between these bounding boxes along one axis, the algorithm reduces the number of necessary checks by only testing overlaps on the other axes if an overlap occurs. Sorting the AABBs using quicksort initially, it then efficiently handles small adjustments using insertion sort as particle positions change, detecting new interactions or ending existing ones based on the relative positions of bounding box bounds. This spatio-temporal coherence makes it a computationally efficient approach for large-scale simulations [40]. Figure 14 shows the way in which the overlap is visualized by YADE.

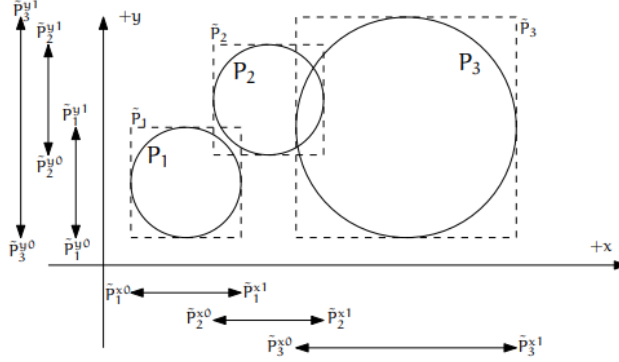


Figure 14: Sweep and Prune algorithm contact overlap detection[40]

To summarize, the Sweep and Prune algorithm organizes particles' bounding boxes by sorting them along one or more axes. It "sweeps" through these sorted lists to identify overlapping boxes, thus determining potential collision pairs. By focusing collision checks only on these active pairs, the algorithm significantly reduces the computational effort [40].

Once contacts are detected, the resolution phase involves computing the forces at these contact points and updating the particle states accordingly. YADE utilizes various contact laws to calculate these forces, such as the before mentioned `Law2_ScGeom_MindlinPhys_Mindlin()` contact law [40]. The normal force is determined by the overlap between particles, while the tangential force accounts for the history of sliding and frictional interactions. These forces are then applied to the particles, updating their velocities and positions through numerical integration methods provided by engines like `NewtonIntegrator()`.

In summary, YADE's approach to contact detection and resolution integrates spatial partitioning, geometric algorithms, and sophisticated contact laws to model particle interactions with high precision. This comprehensive framework ensures that the physical behavior of particles is accurately represented, allowing for realistic simulations of granular materials and discrete systems. Understanding these processes is essential for setting up effective simulations and interpreting the results, making contact detection and resolution fundamental aspects of YADE's simulation capabilities.

2.6.5 Material models

In YADE, material models are fundamental components that define the mechanical behavior of particles and interactions within a discrete element simulation. Materials in YADE are characterized by a set of physical properties, including density, Young's modulus, Poisson's ratio, friction angle, and cohesion, among others. These properties are encapsulated in material classes, such as `FrictMat`, `CohFrictMat`, and `ViscElMat`, each tailored to specific types of interactions and material behaviors. Once defined, materials are assigned to particles or facets in the simulation. Interactions between particles are governed by interaction laws, which use the properties of the assigned materials to compute forces and displacements [40]. For example, common interaction laws used in this study utilize the frictional properties defined in `FrictMat` to calculate normal and tangential forces during contact. Drilling involves complex particle-to-particle and particle-to-tool contacts, where friction plays a key role in defining the interaction between the drilling bit and the surrounding material. `FrictMat` provides essential properties such as friction angle, density, Young's modulus, and Poisson's ratio, which are critical for accurately simulating the resistance and deformation that occur during drilling, which is why this material class is chosen for the numerical model. Figure 15 below illustrates how the `FrictMat` material class interacts with contact law functors during simulations, demonstrating the calculations of forces and displacements in particle interactions.

2.6.6 Optimizing computational time

Simulations have many limiting factors and can become very computationally expensive and long which is why certain advanced techniques are used to optimize computational time. One of

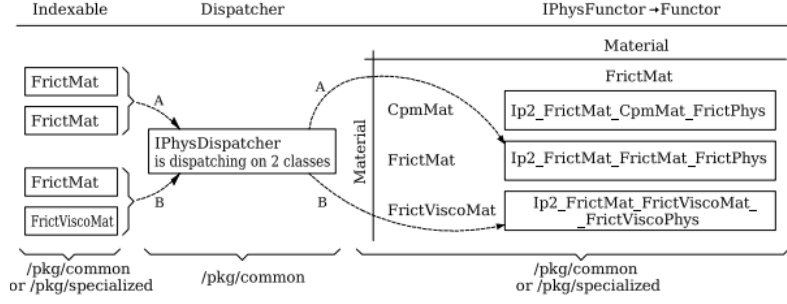


Figure 15: Interaction model of physics functors in YADE [40]

the key aspects of these techniques is the manipulation of the time step to ensure numerical stability while optimizing computational performance. In Yade, the time step is often set to $0.8 \times PWaveTimeStep()$. The P-wave time step is calculated based on the elastic wave speed (P-wave speed) in the material and the smallest element dimension in the simulation [36]. The P-wave speed v_p represents the speed at which compressional waves propagate through a material and it is derived from the material's Young's modulus, Poisson's ratio, and density, using the formula:

$$v_p = \sqrt{\frac{E(1 - \nu)}{\rho(1 + \nu)(1 - 2\nu)}} \quad (17)$$

Once the P-wave speed is known, the P-wave time step $\Delta t_{P\text{-wave}}$ is calculated by considering the smallest dimension of the particles in the simulation. This time step is chosen to ensure that the wave does not travel further than the smallest particle during one-time step, which is crucial for numerical stability [36]. The P-wave time step is then expressed as:

$$\Delta t_{P\text{-wave}} = \frac{\text{smallest-particle-size}}{v_p} \quad (18)$$

This ensures that the time step is small enough to accurately capture the dynamic interactions between particles but large enough to minimize computational time. By setting the time step to 80% of the calculated P-wave time step, Yade balances precision and efficiency, preventing numerical instabilities that could arise from larger time steps.

The time step in simulations must be less than the time it takes for a wave to propagate through the material to ensure numerical stability and accurate particle interactions. A larger time step could allow a wave to travel across multiple particles within a single step, leading to inaccuracies in force calculations and potentially unstable simulations. By maintaining a smaller time step, the simulation can accurately capture dynamic interactions and transient effects, resulting in more realistic behavior of the material.

2.7 Simulation stability and coordination number

The coordination number represents the number of nearest neighbors surrounding a given particle in a system. It quantifies the degree of connectivity within a granular material or lattice structure, providing insight into the arrangement and interaction of particles. A higher coordination number typically indicates a more stable configuration, as it suggests greater inter-particle contact and stronger overall structural integrity [34]. Understanding the coordination number is essential for predicting the behavior of granular assemblies under various loading conditions, as it affects how forces are transmitted through the material and how it responds to external influences.

The coordination number is defined by the following equation:

$$Z = \frac{2C - N_1}{N - N_1 - N_0} \quad (19)$$

where C represents the total number of contacts, N the number of particles, and the 2 accounts for the fact that each contact is shared by two particles. N_0 is the number of particles with no contacts and N_1 is the number of particles with only a single contact, which are subtracted since they do not contribute to the stability of the system. A granular system with $Z=4$ is considered an isostatic system, meaning that the number of constraints and reactions matches the number of degrees of freedom of the system [36]. In YADE, the coordination number calculation is a standardized function that can be called as $Z = \text{yade.utils.avgNumInteractions}(\text{cutoff}=0, \text{skipFree}=\text{True}, \text{considerClumps}=\text{False})$.

2.8 Contact force distribution

In YADE, it is possible to track the contact forces formed between the individual particles of granular beds and plot them to visualize the contact force distributions at specific iterations of the simulation. This is very useful as assemblies with well-distributed contact forces lead to well-developed force chains. The distribution of forces among particles is more uniform, leading to increased stiffness and enhanced load-bearing capacity. When a granular material is subjected to external stress, the presence of these robust contact distributions enables the system to resist deformation more effectively [16]. As a result, granular materials with more distribution of contact forces and well-established force chains can better support applied loads.

3 Experimental study

The following section focuses on the experimental study of drilling aimed at gathering reliable results that can be used as a benchmark for analyzing future simulation data. In this chapter, an experimental procedure is defined to collect data of penetrative and rotating drilling, which will later be used to validate the results of simulations.

3.1 Experiment background

The drill-bug setup at the University of Twente was already introduced in Figure ?? in Chapter 1. This setup faces multiple limitations and challenges. The setup experiences significant frictional losses in the drill bit assembly. These losses are mainly due to granular particles leaking between the drill halves and friction between the guidance plates and drill bit stems, which are designed to prevent oscillation [18]. Additionally, being only in its prototype stages, the drill is not equipped with any sensors or other data collection devices that would make it possible to run adequate experiments. Therefore, the majority of the research needs to be done with the use of simulations. However, the simulation results need to be validated against a certain dataset. This dataset is created by running a set of experiments for which the data is collected and compared to the results of a simulation run with the same parameters. The experiments chosen for the purposes of this research are inspired by K. Vink’s [18] work on the effects of different drill bit geometries on drilling performance. In this study, four different drill bit geometries were created and 3D printed using polylactic acid (PLA) material. The original 3D-printed drill bits are also used in this study. The experiments focus on penetration or dip tests of the aforementioned drill bits into a bed of glass beads representing soil. The goal of the experiments carried out by Vink was to measure the normal force during penetration tests of various drill bits and to compare them in order to determine the most efficient geometry type. The same set of experiments will be repeated to check the validity of the results and the experimental method, while additional experiments will also be carried out to test different types of motion and varying conditions. The experiment plan and setup are laid out in the following section.



Figure 16: Drill bits used in this study

Drill bit	Drill point angle (deg)	Teeth present	Diameter at base (mm)	Cross-section (mm ²)**
Bit V1	15	No	16	159.05
Bit V2	15	No	16	164.06
Bit V3	19.19	Yes	24x16*	214.81
Bit V4	20	Yes	20.99	280.14

Table 1: Drill bit specifications [18]

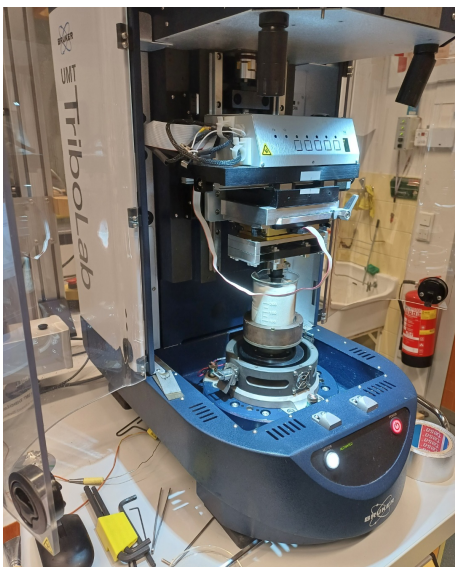
* Elliptical shape

** Measurement is done at maximum penetrating depth (50mm)

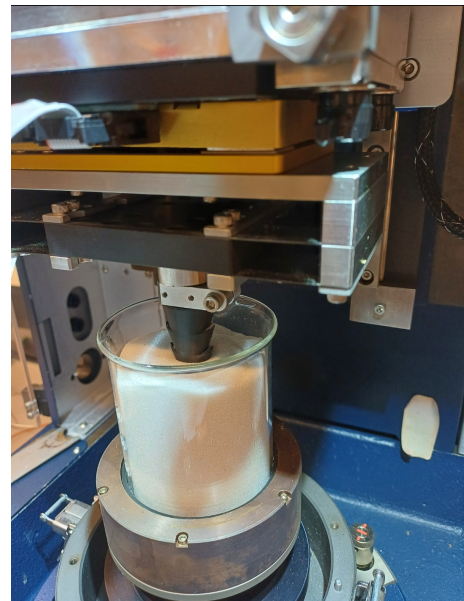
3.2 Experiment method

3.2.1 Experiment setup

The experiment utilizes four distinct shapes of drill bits (V1, V2, V3, V4), each fabricated from PLA using an Ultimaker S5 printer. The drill bits used in these experiments are shown in Figure 16 above, accompanied by Table 1 with their specifications. The granular substrate consists of highly spherical quartz glass beads with a particle size range of 200-300 μm and a density of 2.2 g/cm^3 . Testing is conducted using a Universal Mechanical Tester (UMT) TiboLab, developed by Bruker, which is integrated with a rotating table to provide controlled rotation of the substrate. The UMT is a versatile and precise instrument, capable of simulating a wide range of mechanical testing conditions, making it ideal for this study. Its advanced features allow for precise control over testing parameters, ensuring accurate and reproducible results. A DFH-50G load cell, with a measurement range of 5 to 500 N and a resolution of 25 mN, is employed for precise force measurements. The load cell is highly sensitive and capable of detecting minute variations in force, which is crucial for accurately capturing the dynamics of the drilling process. Its integration with the UMT ensures that both normal and tangential forces can be measured simultaneously, providing a comprehensive understanding of the forces involved. The substrate was originally housed in a container with a diameter of 89 mm and a total volume of 818.45 cm^3 , however, for the rotational tests a special kind of platform was added to the bottom of the UMT. This platform restricts the maximum radius of the container, which is why in these experiments a differently dimensioned beaker is used. The new diameter is 70 mm and the volume is 962 cm^3 . The drill bit is also scaled down by the same factor. A cleaning brush is used to remove residual grains from the drill bits, ensuring that each test starts with a clean bit to maintain consistency. The substrate level is normalized after each experiment by leveling it with a lab spoon. A data acquisition system records force and displacement data throughout the experiment, enabling detailed analysis of the drilling performance. This setup ensures that all relevant data is captured and stored for subsequent analysis, providing valuable insights into the optimization of drilling techniques. Before the experiments begin, the rotational platform attachment is placed on the bottom of the UMT machine and secured with long screws. The beaker is filled with glass beads and placed inside the attachment ring and additionally secured with the use of double-sided tape for extra secure fit. The drill bits are mounted to the attachment of the UMT using the specially designed attachment slots and are tightened in place with the use of an Allen key. The setup is shown in Figure 17 below.



(a) UMT



(b) Rotation attachment

Figure 17: Experiment setup

3.2.2 Procedure

In total, three different experiments were conducted with varying parameters. All three are summarised below for easier understanding:

- **Experiment 1:** Penetration test at different penetration speeds
- **Experiment 2:** Rotations test at different combinations of penetration and rotation speeds
- **Experiment 3:** Penetration test with the presence of water

The primary objective of **Experiment 1** is to collect accurate measurements of normal forces acting on the different drill bits to check the reproducibility and validity of the experimental setup. Independent variables in this study include the drill bit shape (V1, V2, V3, V4) and the drilling speeds (0.2, 0.5, 1, 2, 5, 10 mm/s). The dependent variables measured are penetration force and penetration work, calculated as the product of force and distance during penetration. As briefly mentioned before the preparation involves fabricating the drill bits, filling the container with quartz glass beads to about 70%, and normalizing the surface of the granular substrate before each test. During the experimental setup, the drill bit is attached to the UMT machine using a cylindrical holder with a notch to lock it in place, and the container with the substrate is placed on the rotating table and secured with a ring platform. The load cell is calibrated and aligned to measure both normal and tangential forces, and the rotating table is set to 0 rpm.

Testing is carried out by performing tests for each drill bit at six specified drilling speeds, with three repeats per speed setting. In each test, the drill bit penetrates to a depth of 50 mm into the stationary substrate, holds for 10 seconds to allow the regolith to settle, and then retracts to the initial height. The drill bit is cleaned with the brush before each new test to ensure that all glass residue is removed. Data collection involves recording penetration and retraction forces using the load cell, measuring displacement with the digital readout, and capturing rotational force and torque on the drill bit. Penetration work is computed from the force and displacement data. Data analysis includes calculating the average penetration and retraction forces for each drill bit at each penetration speed, plotting penetration work and pressure, and comparing the results to previously obtained results of the same experiments carried out by Vink [18]. Penetration pressure is normalized with respect to the cross-sectional area of each drill bit.

In **Experiment 2**, a similar procedure is followed as in the previous experiment, except that the lower platform is no longer stationary, but rotating. The goal of this experiment is to measure the normal force exerted on the drill bit during rotational or conventional drilling. Independent variables in this study include the drill bit shape (V1, V2, V3, V4), the drilling speeds (1, 5 mm/s), and the rotational speeds (2, 5, 10 rpm). The dependent variables measured are penetration force and penetration work and pressure, as described in Experiment 1. In conventional drilling the drill bit rotates with a certain angular velocity, however, due to the limitations of the UMT machine, a decision was made to rotate the sand bed instead. This is why the rotation speed was capped at 10 rpm, to prevent excessive movement of the regolith before it is penetrated by the drill. This value was determined by visually observing the movement of the regolith under rotation. The experiment follows the same trajectory penetrating to a depth of 50 mm into the rotating substrate, holding for 10 seconds to allow the regolith to settle, and then retracting back to the original height. For the entire duration of this experiment, the platform is rotating. The results of this experiment are used to identify trends of conventional drilling and compare them to trends obtained later on in drilling simulations.

Experiment 3 is another extension of the penetration experiment created to examine the effects of adhesion on drilling performance. Water is added to the substrate to achieve the desired moisture content by weight and mixed thoroughly to ensure uniform distribution. The experiment is carried out at 20% of water content by weight added to the substrate. Besides the addition of water, the experiment is in fact a simple penetration test carried out at penetration speeds of 1, 5, and 10 mm/s, with each set of measurements repeated three times. This additional study aims to explore how moisture content affects drilling performance due to the effects of adhesion

and capillarity, further informing optimal drilling strategies in varying environmental conditions. Independent variables in this study include the drill bit shape (V1, V2, V3, V4), the drilling speeds (1, 5, 10 mm/s), and the water content by mass percentages (0%, 20%).

3.3 Experiment results and limitations

3.3.1 Experiment 1 - Penetration test at different penetration speeds

The work done was compared for the new and previously performed sets of experiments. In each case, an average of the three test runs was taken, and error bars were plotted to show the upper and lower limits of the tests. In Figure 18, an example result is shown, representing the force vs depth graph of the V1 drill at 10 mm/s in both the original and the new experiments. Here it can be seen that there are a lot of similarities between the two graphs, meaning that the experiments showed good repeatability so far.

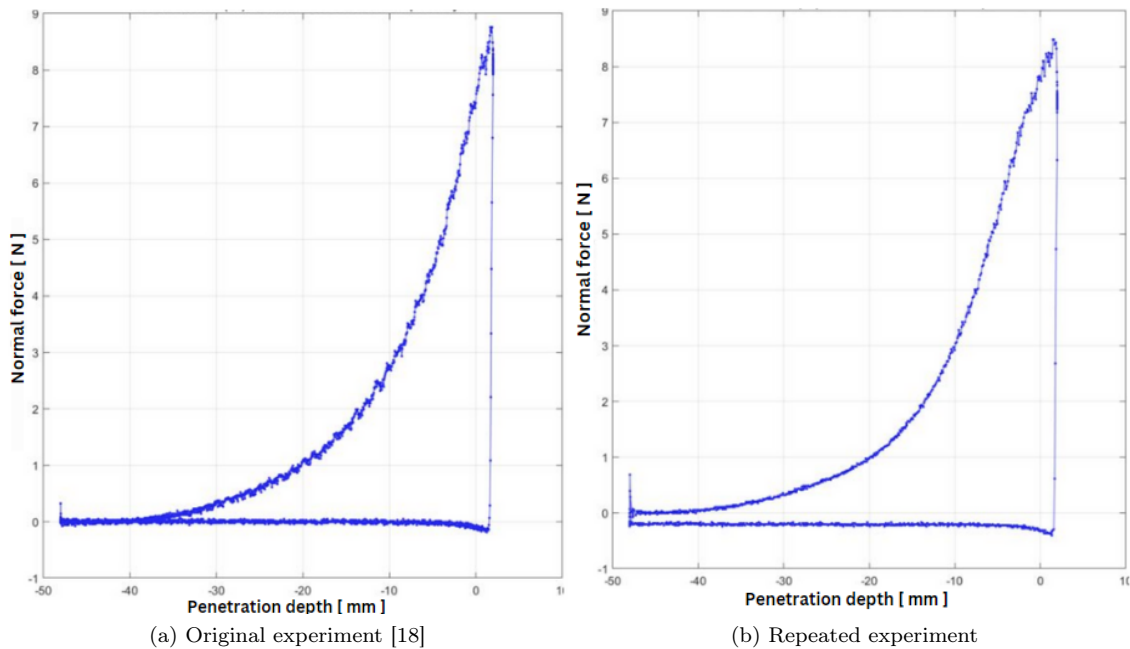


Figure 18: Force vs penetration depth plot for V1 at 10 mm/s

This data shows that as the drill bit penetrates into the substrate, the force gradually increases with its peak being at maximum penetration depth. After retraction, the force rapidly reduces and remains very minimal until it reaches zero once the drill bit is fully retracted, which was also observed in Vink's experiments [18]. The graph shows a clear relationship between penetration depth and normal force. During penetration, the force increases due to the resistance from the compacting sand, while during retraction, the force drops sharply as the pressure is released and the sand structure collapses [21].

Work done is calculated using the trapz function in MATLAB which helps to integrate over force and traveled distance (penetration depth), while the pressure was calculated by normalizing the maximum forces exerted with their respective drill bit area as outlined in Table 1.

Figures 19 and Figure 20 show that there is a good repeatability between the two experiments with minimal differences by looking at the work done during penetration. Smooth drill bits needed the least amount of work to penetrate the substrate, while radially toothed drill bit needed the highest amount of work, as described in Vink's study [18].

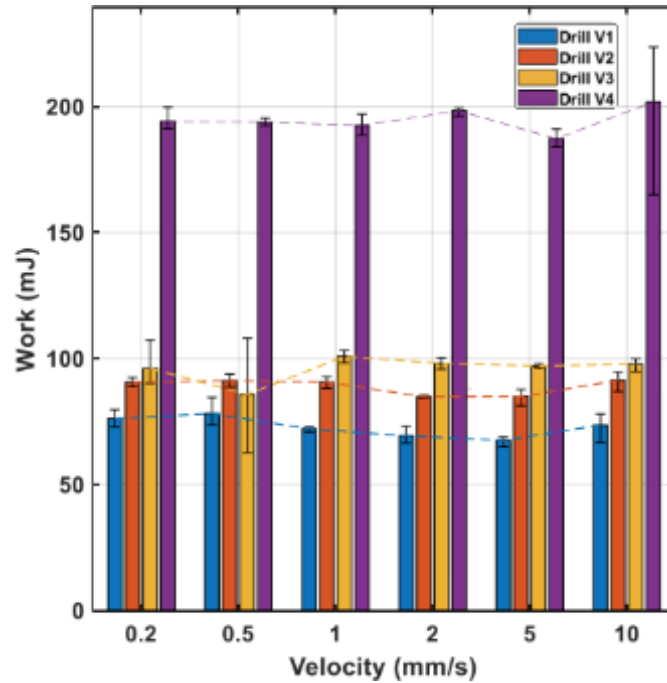


Figure 19: Work during original penetration experiments [18]

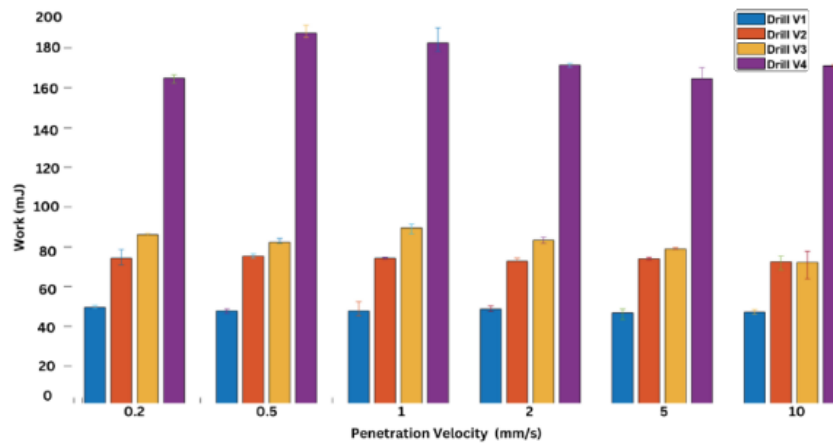


Figure 20: Work during repeated penetration experiments

The same can be observed for the maximum pressure plots shown in Figure 21. This shows that the force of drilling is highly dependent on the drill bit shape, with V4, having radially spaced teeth, showing the highest forces. Since the trends remained unchanged and there is only a small difference in values, the experimental setup and method are deemed correct.

The slight disparity between the compared results could occur due to multiple reasons. Potentially, the way in which the substrate is leveled after each test can differ since the leveling is done manually with different forces applied. If the substrate is leveled and pushed down with a higher force, it can compact it and make it slightly more difficult to penetrate. Another consideration is the time of the year in which the experiments were conducted. The original experiments took place in the winter of January, while the new ones were executed in the spring season in May. In humid

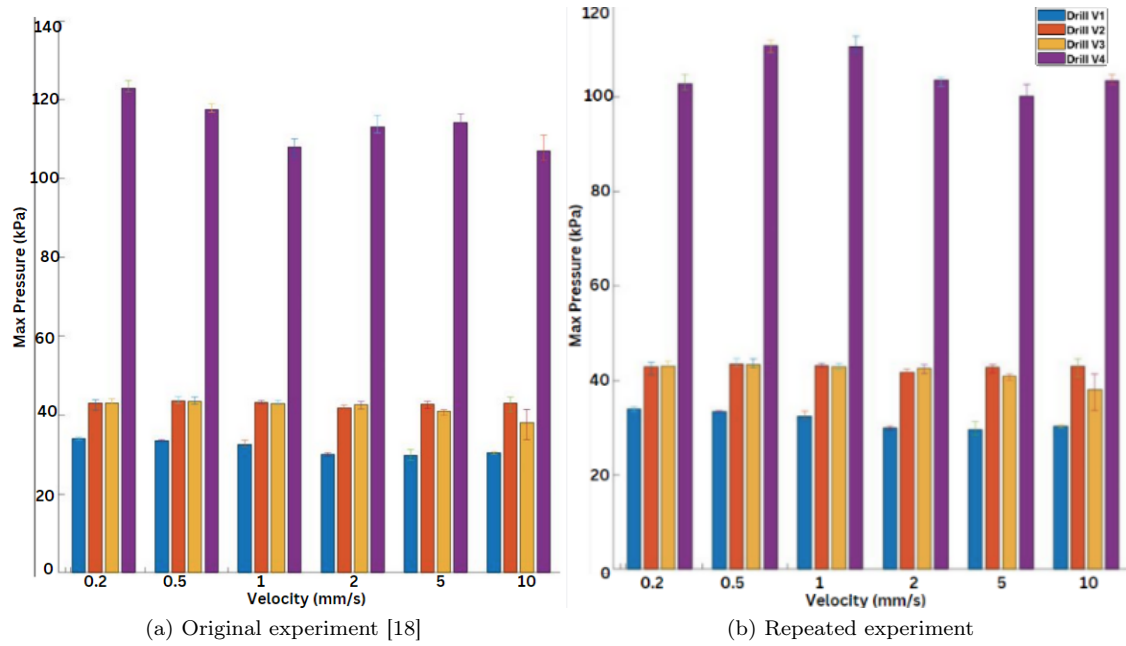


Figure 21: Maximum pressure for penetration experiments

environments, the particles of sand can trap water particles between them, and in colder weather, there is less evaporation of the trapped water particles. A higher level of water in the system can make it harder to penetrate the substrate, resulting in an increase of the penetration force needed.

3.3.2 Experiment 2 - Rotation test at different combinations of penetration and rotation speeds

With the addition of rotation in the system, the following results were obtained as outlined in Figures 23 and 24. Figure 22 shows an example result obtained for the drill bit V1 at 5 mm/s, rotating at 10 rpm

It is clear that increasing the rotational speed for each penetration speed significantly reduces the needed penetration force, which is in line with the principle of rotational drilling outlined in Chapter 2. Rotational drilling reduces the required axial (penetration) force by introducing torque, which generates a shearing effect at the drill bit's cutting edges. The torque creates lateral forces that help break apart the material and reduce the material's resistance to penetration. This shearing action distributes the load more evenly, allowing the axial force to be lower than in pure penetration drilling, where all the force is concentrated vertically [11]. Additionally, rotation helps clear debris and minimizes friction, further decreasing the overall force needed for effective drilling.

Adding more motion into the system has easily fluidized the granular bed, creating more motion of the particles and breaking apart the contact chains between them. As postulated in Chapter 2.8, higher disturbances to the contact force distribution will allow for less resistance of the granular bed during drilling. This is why the drill bits rotating at higher speeds require less work and generate less pressure.

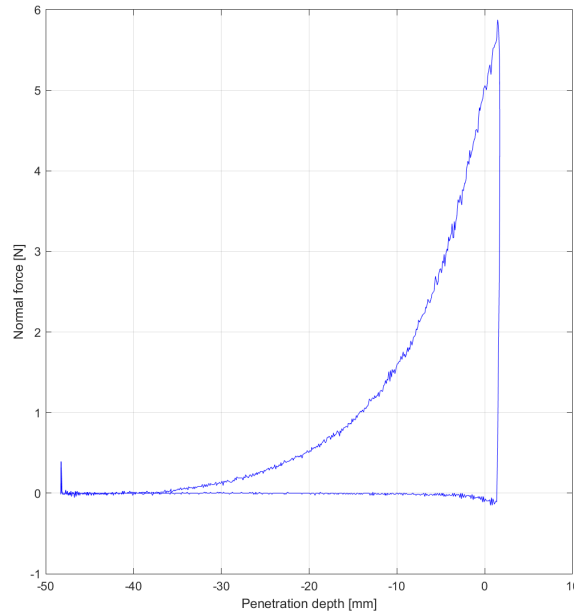


Figure 22: Force vs penetration depth plot for V1 at 5 mm/s and 10 rpm

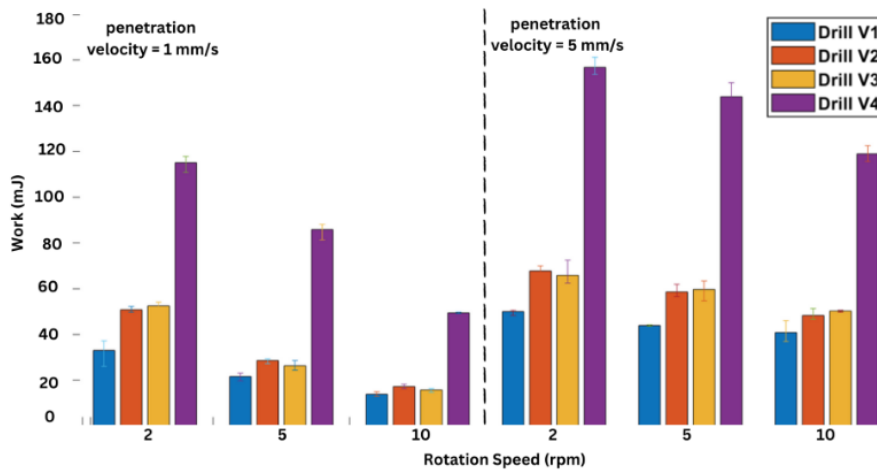


Figure 23: Work during rotation experiments

An interesting phenomenon is observed that a combination of higher rotating speed and higher penetration speed is less effective (requiring higher penetration force) than using a slower penetration speed. This may seem counterintuitive. At the granular scale, materials often exhibit viscoplastic behavior, meaning their deformation and flow depend on both the applied stress and the rate at which it is applied [10]. At slower penetration speeds, the drill has more time to shear the material with each rotation, leading to more efficient material removal and reduced penetration force. Faster penetration speeds force the drill bit to remove more material in a shorter amount of time, which can exceed its shearing capacity. As a result, the bit struggles to efficiently shear the material, leading to increased resistance. This also generates more friction between the bit and the material, which further impedes cutting performance and requires greater force to continue drilling. [4]. Finally, slower speeds allow for smoother interaction between the drill and material, reducing vibrations and binding, while giving the torque more time to act on the material.

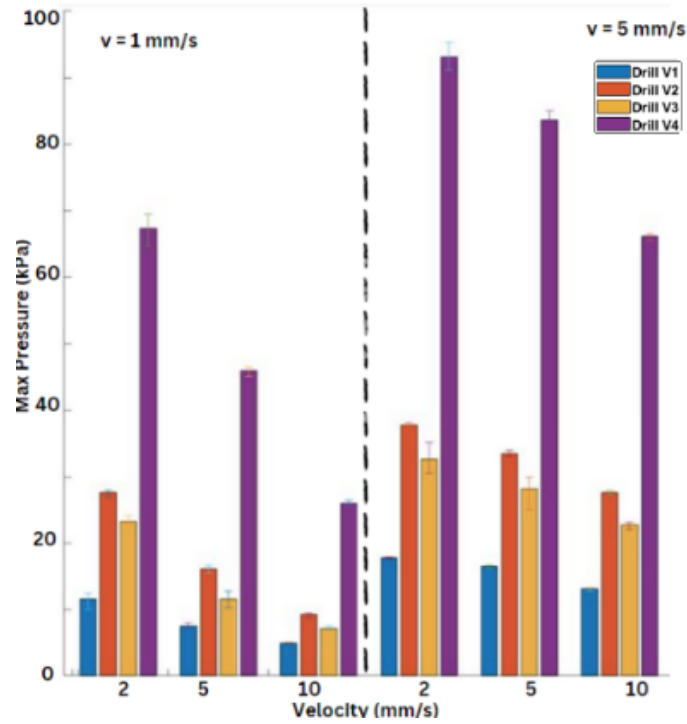


Figure 24: Maximum pressure during rotation experiments

3.3.3 Experiment 3 - Penetration test with the presence of water

For the final experiment, the contents of the cylindrical beaker were measured and water weighing 20% of the mass of the grains was added to the beaker. The glass beads and the water were mixed until an even substance was formed and the experiments continued in the usual manner. An example measurement for drill bit V1 at 10 mm/s is shown in Figure 25 below.

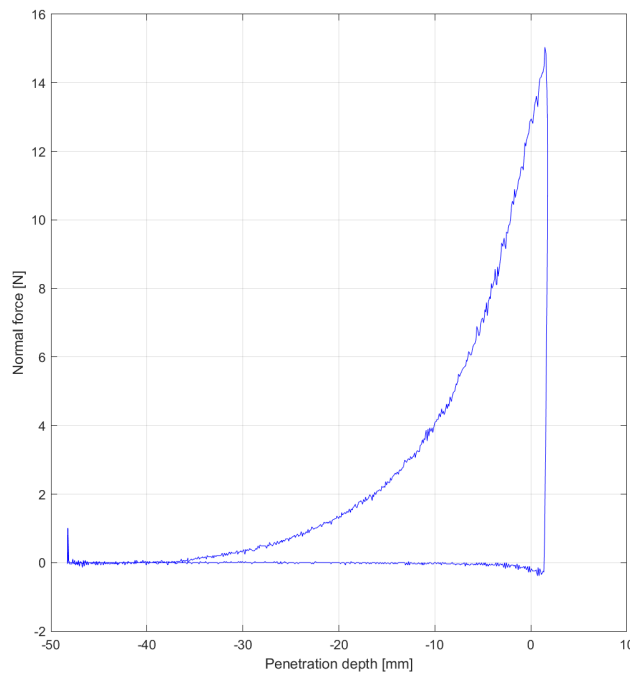


Figure 25: Force vs penetration depth plot for V1 at 10 mm/s

For the results presented in Figure 26 and 27, it can be observed that higher levels of water in the substrate lead to much higher penetration forces required for drilling. This was expected as wet soil requires more penetration force than dry soil because the presence of water increases the cohesion between soil particles and adhesion with the drill bit. Chemically, water and glass beads form a compound known as silanol. Silanol has relatively strong Silica-Silica bonds between the glass interfaces, making it more difficult for a drill bit to penetrate [41]. Additionally, the increased moisture can create capillary forces that further resist the penetration of the drill. In contrast, dry soil has lower cohesion and less resistance, allowing for easier penetration.

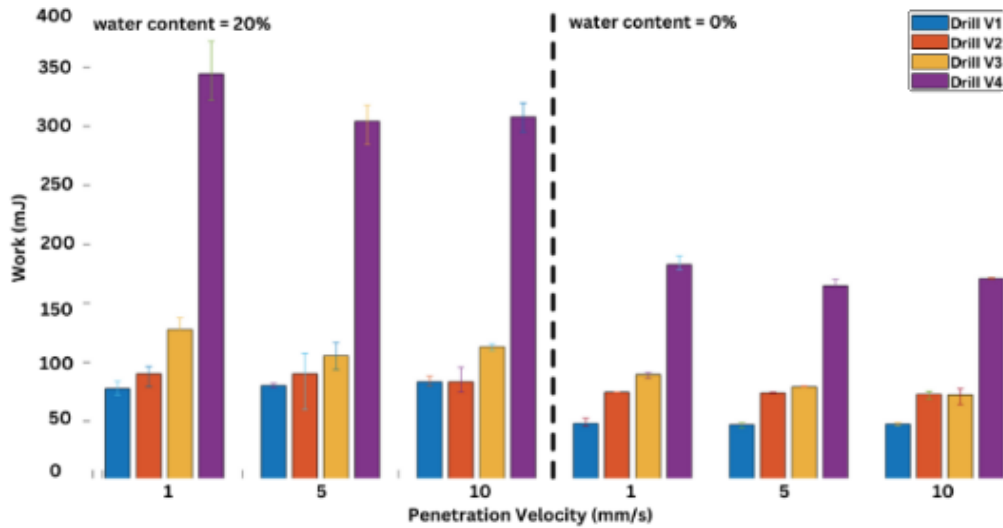


Figure 26: Work of adhesion

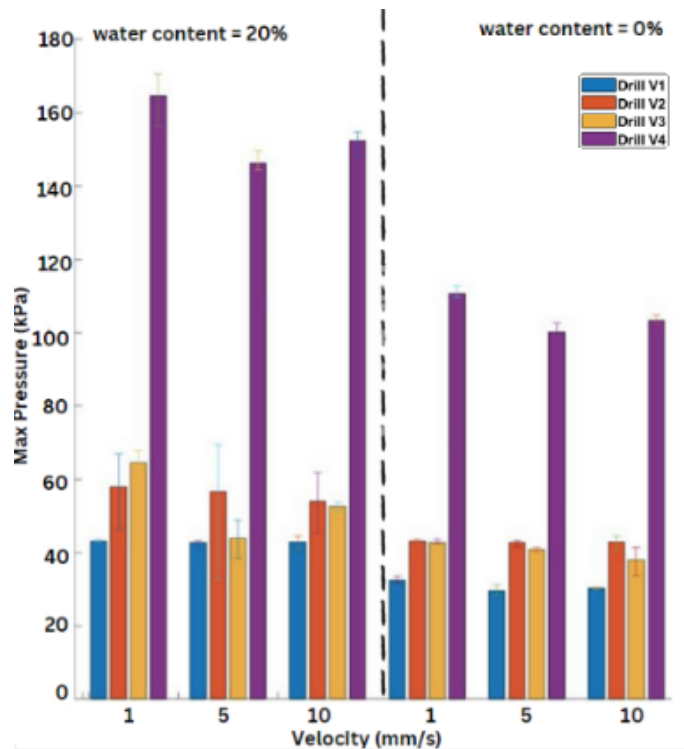


Figure 27: Maximum pressure of adhesion

While the results obtained with this experiment show a satisfactory trend, there are a few limitations that need to be addressed to further interpret the obtained results. The first consideration is that the water content was not controlled throughout the experiment. Glass beads do not mix well with water, and water tends to fall through between the particles and settle at the bottom of the cylinder after a certain time. During the experiment, the substrate was mixed with a spoon multiple times, but it was difficult to guarantee uniform distribution of water for the whole duration of the tests. After the initial mixing, no more water was added to the system, therefore any subsequent evaporation was unaccounted for. Another consideration is the adhesion between the wet glass particles and the drill bit. Between each test, the drill bit was cleaned with a brush. The cleaning had to be performed with care, in order to not disrupt the calibrated load cell, meaning that not a lot of pressure could be applied on the drill bit. This made cleaning a lot more difficult, resulting in the drill bit not being properly cleaned before each test. This is especially true for the drill bit V2, where the small slot would get clogged by wet substrate, which was difficult to remove. Hence, the numerical values obtained from this experiment should be treated with more care.

The experiments were successful in demonstrating reproducibility and providing new insights into drilling performance under various conditions. Experiment 1 confirmed the reliability of the experimental setup, showing consistent results with minimal variation from previous studies. Experiment 2 supported the theoretical principles of rotational drilling, revealing a significant reduction in penetration force with rotation and highlighting the complex interplay between material removal, shear forces, and friction, including the counterintuitive increase in force at higher rotational and penetration speeds. Experiment 3 demonstrated that the presence of water increases penetration force due to heightened cohesion and adhesion within the substrate, despite challenges such as uneven water distribution and difficulties in cleaning the drill bits. Overall, these experiments establish a robust foundation for further research and simulation validation, particularly for scenarios like dual reciprocation drilling that cannot currently be tested at the University of Twente.

4 Numerical modelling of drilling

In this chapter, we delve into the numerical modeling of the drilling process, detailing the setup of the model and the methodologies used for performing calculations. The first section outlines the development of the model, highlighting key assumptions, input parameters, and computational strategies employed. This is followed by a sensitivity study, where various parameters are systematically altered to assess the model’s response and its alignment with theoretical expectations. Finally, a validation study is conducted to compare the simulation results with experimental data, determining the model’s accuracy and reliability in replicating real-world drilling behavior.

4.1 Model setup

Before the data gathered with this model can be used in further analyses, it is necessary to check the validity of the model itself. This is done by varying certain simulation input parameters and observing if the output forces behave as it would be expected, according to theory. Since this requires running many simulations, a scaled-down version of the model is applied, to speed up the computation time. Therefore, all the dimensions used in the experimental setup described in the previous chapter, are now reduced by five times. A simplified cone geometry was used to mimic the drill bit. This was done using cone facet functions in Yade, instead of importing STL files. Using the 'facetCone' function in YADE is beneficial because it directly creates a simplified and optimized geometry within the simulation, avoiding the complexity and overhead of importing and processing detailed STL files. This reduces computational load and memory usage, as YADE facets are more efficiently handled by the simulation engine than the typically high-resolution and detailed mesh data in STL files. Once all the necessary geometry is added to the simulation, simplified material is assigned to each body. This material has a low elastic modulus E which reduces the computational time. The material is assigned to both the substrate and the drill bit, while the cylinder uses the O.material’s default properties as these properties will remain unchanged during the sensitivity study. A common value for the coefficient of friction between the drill bit and the substrate is assigned, as well as a moderate damping coefficient [27]. In YADE, the damping factor controls energy dissipation, stabilizing the system by reducing kinetic energy over time. It mimics the effects of friction, drag, or resistance forces that slow particle motion. The value used in this study is commonly chosen in DEM simulation as it strikes a balance between energy dissipation and maintaining realistic particle dynamics [36]. All the described parameters and the simulation’s domain size for the duration of this study are defined in Table 2 below.

Parameter	Value
Drill diameter	3.2 mm
Drill length	14 mm
Domain (cylinder) height	50 mm
Domain (cylinder) radius	7 mm
Elastic Modulus	100 KPa
Poisson’s ratio	0.3
Density	1000 kg/m ³
Coefficient of friction	0.577
Damping coefficient	0.4
Particle size	0.3 mm
Penetration speed	10 mm/s

Table 2: Test material parameters

Finally, the substrate is added to the simulation by the use of a sphere pack function which fills the space of the cylindrical facet with a packing of spheres with a constant radius of 0.3 mm. Once the bodies have been defined, the necessary physical laws and models need to be assigned. As already discussed in Chapter 2, a list of engines is compiled to detect collisions and apply contact laws. In this case, Hertz-Mindlin contact laws are applied. Next is the definition of the motion function. The motion function is defined in such a way that it mimics the motion of the drill bit in the experiments. The drill bit moves downwards with a velocity of 10 mm/s and penetrates 10 mm into the substrate, where it waits for 10 seconds before being retracted at the same speed. In the

case of penetration drilling, this can be achieved by using YADE's Translation engine, however, once rotation drilling is examined, this engine needs to be coupled with another engine that defines rotation. The motion is offset to start only after a certain number of iterations ($O.iter = 5000$) to allow time for the particles in the sphere packing to distribute and relax in the cylinder. For easier understanding, Figure 28 describes the path of the drill bit during the drilling action of both pure penetration and penetration with rotation. This drill bit motion plot is then compared to that of a reciprocating drill bit in Figure 29. This motion function is applied to all further simulations. Note that the motion plot shown here is for the real domain size, however, the shape remains the same for the down-scaled version.

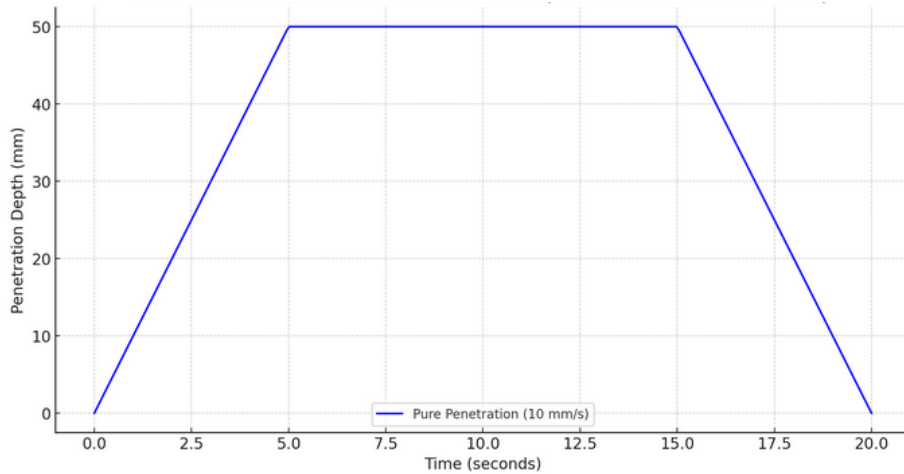


Figure 28: Drill bit motion plot (penetration and rotation)

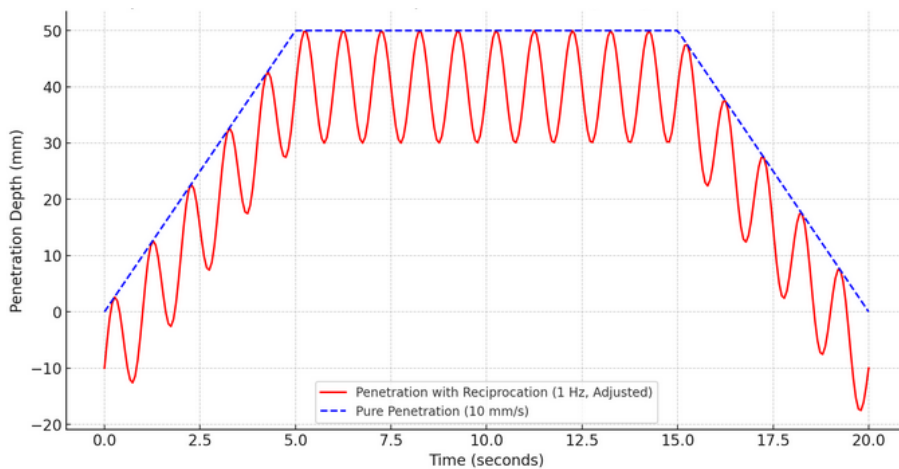


Figure 29: Drill bit motion plot (reciprocation)

The final step is to calculate and track the normal force exerted on the drill bit during the drilling action by aggregating the vertical components of both normal and shear forces from all contact points between the drill bit and the surrounding material. Therefore a conditional block is created that filters interactions to focus on those where one body belongs to the cone and the other body is a separate object (e.g., particles or facets), which are relevant for tracking forces acting on the cone. A line $\mathbf{F}_n += \mathbf{c.phys.normalForce}[1] + \mathbf{c.phys.shearForce}[1]$, is summing the vertical components of the normal and shear forces exerted at each contact point between bodies. Here, $\mathbf{c.phys.normalForce}[1]$ and $\mathbf{c.phys.shearForce}[1]$ retrieve the y-direction components of the normal and shear forces, respectively. By adding these components, the code accumulates the total vertical force (F_n) acting on the cone, which is essential for assessing the interaction between the cone and surrounding particles or facets in the simulation. The computation of normal and tangential forces is carried out as described by Hertz and Mindlin's equations described in Chapter 2.

The `addPlotData()` function is responsible for collecting and logging data related to the simulation, specifically tracking the vertical position of the cone and the forces acting on it. First, it retrieves the current position of the cone along the y-axis from the simulation. Then, it initializes a variable F_n to accumulate the total force acting on the cone. By iterating over all interactions in the simulation, the function identifies those involving the cone and adds the normal and shear forces from these interactions to (F_n) [40]. This force data, along with the current iteration number, the y-position, and the elapsed time since the simulation started, is then passed to a plot for real-time visualization. Additionally, the y-position and force data are appended to lists for later analysis or saving. A `PyRunner` function is set up to collect data after every 100 iterations to reduce redundantly large data sets that will increase the memory issues faced by the computer.

4.2 Sensitivity study

This section investigates the sensitivity of a simulation model by examining how variations in input parameters affect the outcomes. By systematically altering key variables and analyzing the resultant changes, the study evaluates the robustness and reliability of the model. Parameters that have the most effect on the computational cost are chosen for this study, as it is useful to gain insight into how these parameters can be manipulated to reduce the load of the simulation. These parameters include particle size, elastic modulus, coefficient of friction (COF), and penetration speed.

4.2.1 Particle size

In the first sensitivity study, a range of particle sizes was tested to evaluate their effect on the normal force exerted on the drill bit during the drilling process. This was necessary to combat the memory issue with the computer. Namely, in the full-scale model, with the real particle size, the number of particles and the number of contacts is too great. The computer does not have the necessary memory to handle such a high number of contacts. It is therefore needed to assess the effect of changing particle size on the simulation outputs in order to be able to extrapolate the result for larger particle sizes. The study revealed that as the particle size of the substrate increased, the normal force on the drill bit also increased. Hertzian contact theory proposes that as the size of the contacting particles increases, the contact area between them also increases, which results in a higher total force experienced by the drill bit [30]. As it follows from Equation 6, the normal force is proportional to the square root of the effective radius. However, with increasing particle size in a constrained domain size, the total number of contacts reduces since there are fewer particles in the system. The results displayed in Figure 30 show an exponential increase trend. This could follow from an increasingly present boundary effect. As particle sizes grow without increasing the simulation domain, fewer particles can fit in the same space, leading to higher confinement and increased overlap between particles and boundaries. This confinement amplifies interaction forces. Boundary effects are also limiting the higher end of this study, as particle size reaches the scale of the domain size, producing unreliable results. The diameter of the largest particle used in this study is only 1 mm smaller than the radius of the cylindrical domain. This is why the stagnating part of the curve is disregarded in further analysis. This study is nevertheless very useful as it gives insight into the relationship between the normal force and particle size in this model, which will later allow simulations with larger grain sizes which are much easier to compute. The data points presented below are therefore used for further extrapolation which is shown in greater detail in section 4.3.

When discussing the simulation stability considerations and computational effort in Chapter 2, the time step equation shows the dependence between the simulation speed and the smallest diameter in the model. From Equation 18 it follows that increasing the smallest diameter by a factor of 10 would result in a 10-time increase in the simulation time step.

$$T_{phys} = N\Delta t_{P-wave} \quad (20)$$

Following the Equation 20, the physical time of the simulated action T_{phys} must remain the same, resulting in a 10-time decrease of N , the number of iterations needed [36]. This relation shows how the manipulation of particle size can significantly reduce the running time of a simulation.

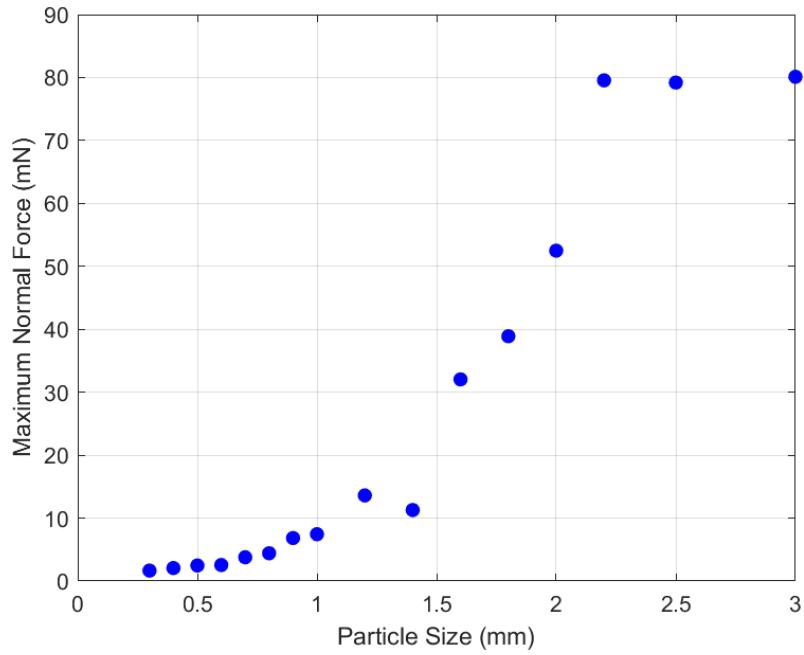


Figure 30: Maximum normal force at different grain sizes

4.2.2 Elastic modulus

In the sensitivity study examining the effect of varying elastic modulus on the normal force exerted on the drill bit, the elastic modulus E is no longer kept the same for both bodies. The value of E of the substrate was kept constant, while E of the cone was varied to check whether expected trends in the normal force were observed.

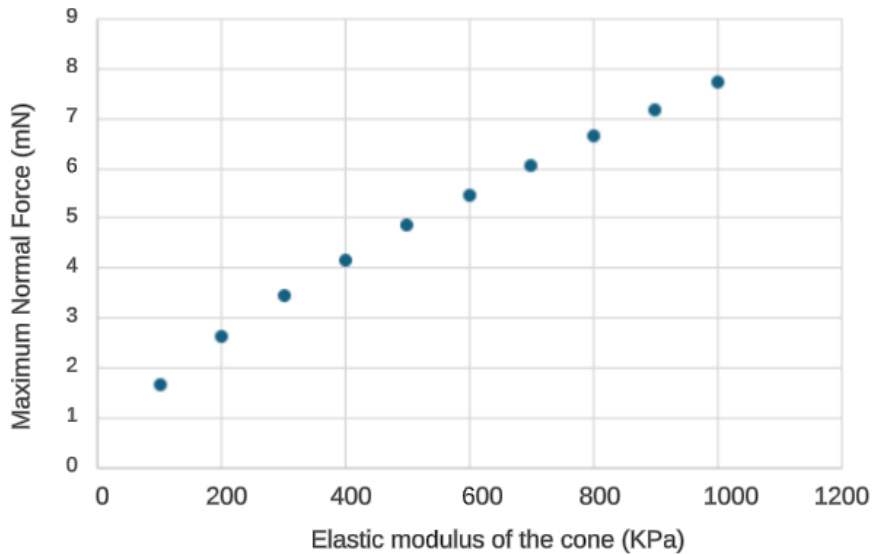


Figure 31: Maximum normal force at different elastic moduli

As mentioned in Chapter 2.2, the reduced elastic modulus described by equation 7 increases as the E value of one of the contacting bodies increases. With a higher reduced modulus, there is an expected rise in the normal contact force recorded as the normal force is directly proportional to the value of E^* . This is sufficiently demonstrated in Figure 31.

4.2.3 Coefficient of friction

The third sensitivity study looked at friction between the drill bit and the substrate by testing the effect of a varying coefficient of friction of the substrate on the normal force recorded. The coefficient of friction is related to the friction angle by a trigonometric correlation. This is the angle made by the resultant of the normal force and the frictional force with the normal force. It is the angle at which an object starts to move when an increasing force is applied parallel to the surface [30]. The relationship between the coefficient of friction (μ) and the friction angle (θ) is given by:

$$\mu = \tan(\theta) \quad (21)$$

By controlling the friction angle in the numerical model, we can change the value of the COF. With the increase of the coefficient of friction, it can be expected that a higher force is needed by the drill bit to penetrate the substrate, due to the substrate's increased resistance to sliding [30], as demonstrated in Figure 32.

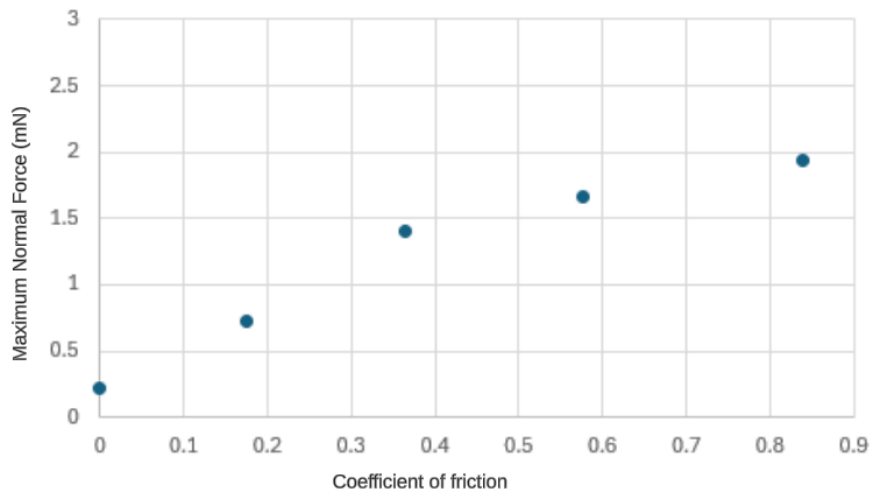


Figure 32: Maximum normal force at different substrate coefficients of friction

The initial increase in normal force with the increasing μ reflects the behavior described by Coulomb's friction law, where an increased coefficient of friction leads to greater frictional resistance [30]. When the friction coefficient of the sand increases, the resistance to movement increases as well and to overcome this increased resistance and maintain the same level of drilling efficiency or to achieve the same penetration rate, the drill bit must exert more normal force on the substrate. Hence, the measured normal force increases with a higher friction coefficient. Equation (11) shows Coulomb's friction law where μ is the coefficient of friction and F_n is the normal force.

$$F_{\text{friction}} = \mu \cdot F_n \quad (22)$$

This graph shows only the realistic values of the coefficient of friction. If the contact angle keeps increasing, the COF reaches very high values, which are never occurring in nature. In these cases, the normal force will start to converge towards a maximum value and the graph stays mostly flat beyond this point.

4.2.4 Penetration speed

In the experiments, it was observed that varying the drilling speed did not have any significant effect on the outcome of the drilling force. This was tested again with the use of the model and the results are displayed in Figure 33. This study is useful as it gives insight into how the simulation speed can be used to minimize computational costs, by manipulating the speed of drilling.

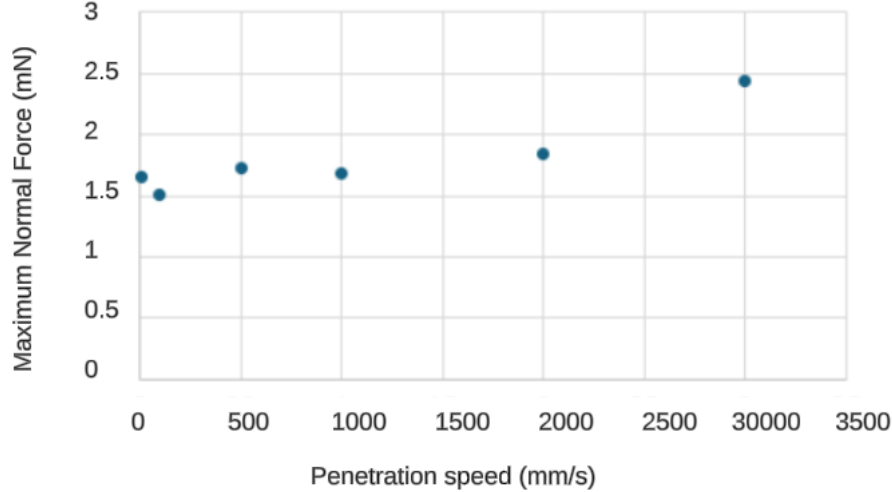


Figure 33: Maximum normal force at different penetration speeds

In the simulations, there appears to be a limit after which the normal force begins to increase with the increasing penetration speed. Therefore for sufficiently low speeds of penetration, there is no significant effect on the normal force. This means that a slightly higher speed can be used in the model, as opposed to the experiment, with the goal of reducing the computational time. To further analyse this phenomena a closer look at the contacts between the substrate particles is needed. For this, a comparison between the penetration speeds at 0.1 m/s, 1 m/s, and 3 m/s is made. As described in Chapter 2, the coordination number is the average number of contacts or interactions a particle has with its neighboring particles in a granular system. The coordination number (Z) at lower speeds (0.1 m/s and 1 m/s) is almost identical with values of $Z=4.21$ and $Z=4.23$ respectively. However at the highest speed (3 m/s) the value of Z increases significantly to $Z=4.79$. An increase in the coordination number indicates that jamming or interlocking of particles is present and the substrate starts to exhibit an increasing resistance to penetration. At lower speeds, particles have more time to rearrange and settle after a disturbance, but at a certain point, the number of contacts increases significantly causing them to interlock [34]. Overall, studies have determined that granular systems that have coordination numbers higher than 4 experience high levels of particle interlocking and jamming [25].

As discussed previously in section 4.2.1, Equation 20 relates the physical time of an action being simulated, to the time step and the number of iterations. If a change in the physical time of the simulation has no significant impact on the outcome, it can be used to reduce the number of iterations and the time step necessary. This is another way to improve the computational efficiency of a simulation.

4.3 Simulation validation

The sensitivity study confirmed that the proposed model behaves in expected ways and according to the theory, and it has provided information on how to further optimize the model's parameters for easier computation. This means that changing certain parameters does not produce significant numerical artifacts and the plotted trends can be used with confidence. The final step is to produce a real-scale simulation that is representative of the experimental setup described in Chapter 3 and to compare the results obtained by each method. For this, updates to the model were made.

The first change is that the domain size is returned to its original state as defined in the experiments. For the validation, a set of experiments was chosen to represent the penetration and rotation tests of the different drill bits. This required an adequate STL to be imported in the simulation, the same file that was used for the 3D printing of the drill bit. Once all the bodies were defined in the model, realistic material properties had to be assigned. All the relevant parameters of the real scale model are shown in Table 3 below.

Parameter	Value
Drill diameter	16 mm
Drill length	70 mm
Domain (cylinder) height	200 mm
Domain (cylinder) radius	7 mm
PLA Elastic modulus	40 GPa
PLA Poisson	0.3
PLA Density	1500 kg/m ³
Glass Elastic modulus	70 GPa
Glass Poisson	0.3
Glass Density	2200 kg/m ³
Coefficient of friction	0.577
Particle size	0.003 m

Table 3: Realistic material properties

As mentioned during the sensitivity study using the particle size of 0.0003 meters is not possible since the number of particles in the simulation becomes so high that the computer does not have enough memory to process the interactions between all of them. This is why a new particle radius was introduced at 10 times the size of the original. This is where the sensitivity study of particle sizes becomes crucial. The sensitivity study concluded that an increasing particle size will result in higher normal forces during drilling. This trend can be modeled as a function that can be used to extrapolate the results when using larger particle sizes in the simulation. For this, a MATLAB code is used to fit an exponential curve to the obtained data. Only the increasing region of the curve in Figure 30 is used for this model, as the flattening of the curve is a limitation imposed by a downsized domain that limits the number of particles in contact at larger grain sizes. Such limit is now shifted to much bigger particle sizes which are not relevant for the chosen size of 0.003 meters.

The MATLAB code fits an exponential function to a given data point by defining an initial model with parameters and then using the `lsqcurvefit` function to optimize these parameters for the best fit. It starts by specifying an exponential function and an initial guess for the parameters. The curve-fitting process adjusts these parameters to minimize the difference between the function's output and the actual data point. After determining the best-fit parameters, the code extrapolates the function to predict values for new x-values and visualizes the results by plotting the original data point, the fitted exponential curve, and the extrapolated value. In this case, the x-values are the given grain sizes and the y-values are the normal force. The fitted exponential function is shown in Figure 34 below.

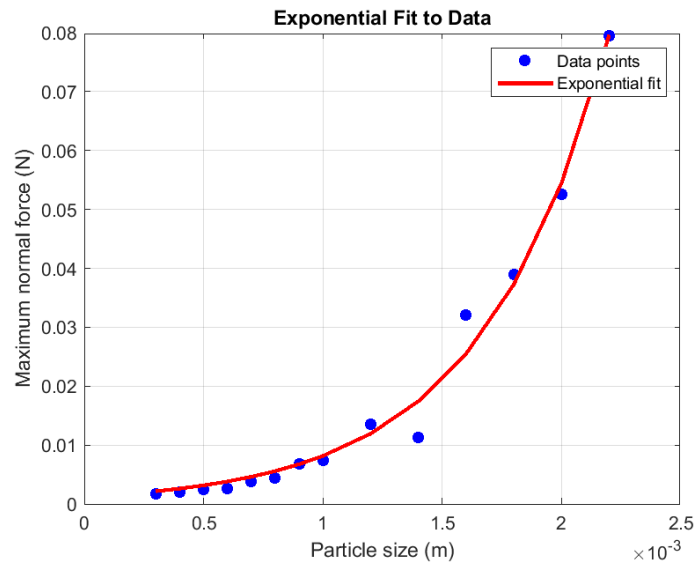


Figure 34: Extrapolation of the normal force of the penetration simulation

The upgraded simulation was run with the same parameters as the experiments, except for the particle size of 0.003 meters. The first test was done using the drill bit shape V4 in two scenarios: 1.- penetration at 10 mm/s and 2.- penetration at 5 mm/s with rotation speed of 10 rpm. The third test was done using drill bit V1 with penetration at 10 mm/s. The results obtained in these simulations were extrapolated using the plot in Figure 34 for the real particle size value. These results are then compared to those of the experiments from Chapter 3. Since three experiments were run for each measurement, an average value of the maximum normal force is taken for each test in this comparison. The results of these comparisons are displayed in Table 4 below, along with the percentage difference between the experimental and simulation values.

	V4-Penetration	V4-Rotation	V1-Penetration
Experiment result	13.02 N	9.6 N	8.4 N
Simulation result	601 N	359 N	394 N
Extrapolated result	14.14 N	8.45 N	9.27 N
Difference	+8%	-12%	+10%

Table 4: Comparison between simulation and experiment results

A difference between the simulation results and the experimental results was to be expected. This is due to many differences and approximations taken in the model. For example, the values of coefficients of friction, damping, and material properties were taken from literature and may not match the real values perfectly. Additionally, the time step can affect the numerical accuracy and the data collecting functions, which run at each 100 iterations and may miss valuable data. The way in which YADE works may not be completely accurate either, as the contact models compute the interaction in a more efficient way that may differ from reality. Effects such as air moisture and temperature are not accounted for in the numerical model either. Boundary effects may also play a more significant role in this study. However, from Table 4 it follows that the results match closely, with less than 15% difference in each case. Therefore, the simulation is regarded as validated and can be used for further testing and research. In the following section, a small parametric study is carried out. The model is altered to simulate different types of drilling motion, with the ultimate goal of investigating the effectiveness of reciprocating drilling in contrast to conventional drilling methods. Additionally, an attempt is made to investigate the effects of capillarity on drilling by simulating the conditions found in Experiment 3 where drilling is done in a wet substrate.

4.4 Parametric study

Now that a working numerical model of drilling has been developed, the next step is to extend that model to, in various ways, gain insight into different parameters of drilling. This can be a series of simulations with different types of drilling motions and varying substrate conditions, that cannot be replicated by any experiments at the moment. In this section, the optimization of the numerical model is made to facilitate dual reciprocation and to test drilling in varying conditions, such as the presence of capillary forces in wet soil.

4.4.1 Modelling dual reciprocation

The first step to creating dual reciprocating motion is to design an adequate drill bit. The same drill that was used in the previous two models is redesigned in SolidWorks. The new drill is created by splitting the original drill bit into two equal halves with a distance of 1 mm between them as shown in Figure 35.

A crucial aspect of this simulation is the modeling of the reciprocating motion of the cone halves. This is controlled by a state machine implemented in a `simple_controller()` function. The motion of the cones is governed by a sinusoidal function that varies with time, creating a reciprocating effect. The simulation starts with the state set to `'move_down'`, triggering the downward motion of the cones. The velocity of each cone half is then adjusted based on a sinusoidal function of time, defined as:

$$v = v_{\text{average}} \pm df \cos(ft) \quad (23)$$

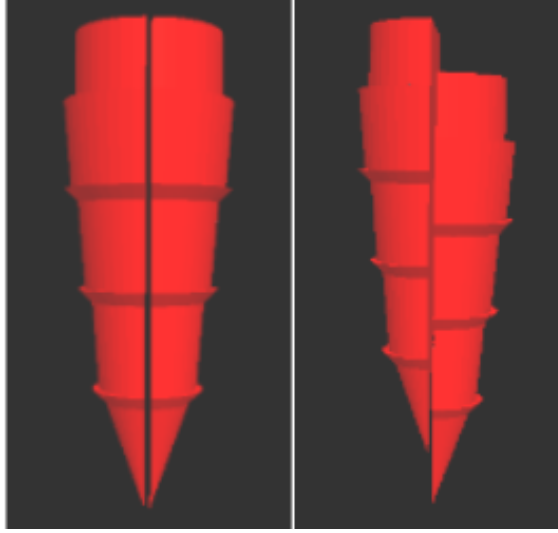


Figure 35: Dual reciprocating motion drill bit positions

Here, $v_{average}$ is the base speed corresponding to penetration speed, d defines the amplitude of oscillation, f controls the frequency of the oscillation, and t is the simulation time. This creates a time-dependent velocity that varies sinusoidally. During the **'move_down'** state, the cones move downward until one reaches a certain position threshold, representing a 50 mm penetration depth, at which point the state transitions to **'wait'**. In this state, the motion stops, and the simulation pauses for 10 seconds. After the wait, the state changes to **'move_up'**, where the velocity is reversed to move the cones upward. Similar to the downward motion, the velocity is governed by the same sinusoidal function but in the opposite direction. Once the cones return to their initial positions, the state transitions to **'done'**, and the motion stops. In this manner, it is possible to control the overall downward speed of drilling, while also controlling the frequency of reciprocation.

4.4.2 Effects of adhesion and partially saturated substrate

As already mentioned in the experimental stage of this thesis in Chapter 3, additional studies need to be done to test the effectiveness of different drilling methods in varying soil conditions. Soil is rarely completely dry and prone to trapping moisture at different levels, which is why an experiment was carried out to measure the normal force during penetration drilling at 20% substrate water content. To recreate these conditions in a simulation has proven to be much more difficult. The addition of water creates strong capillary forces that act between each particle. These forces are a phenomenon that is very complex and difficult to control in DEM models. This is why a simplified version was needed in order to run the simulations. A possible solution is to enable adhesion force tracking in the MindlinPhys contact law in YADE and to modify the input parameters to compensate for capillarity.

As mentioned in Chapter 2, adhesion forces can be computed using the JKR theory displayed in equation 24.

$$F_{adh} = -\frac{3}{2}\Delta\gamma\pi R \quad (24)$$

Here R is the radius of the particle and $\Delta\gamma$ is the interaction energy. A simple way to calculate the capillary force is by using equation 25.

$$F_{cap} = -2\pi\gamma_{wa}R\cos\theta = -0.128N \quad (25)$$

Here $\gamma_{wa} = 72mJ/m^2$ is the surface tension of water. A general rule is that the contact angle θ lower than 90° represents a surface that is well coated by a liquid [36]. This is why a value of $\theta = 20^\circ$ was chosen to show the dynamics of a partially wetted surface since fine glass granulate was partially mixed with water.

As only the equation 24 is used in the numerical model, it is necessary to manipulate the $\Delta\gamma$ value to reflect the result of the capillary forces.

$$F_{adh-DEM} = -\frac{3}{2}\Delta\gamma_{DEM}\pi R = -0.128N \quad (26)$$

The γ_{DEM} value to be used in the simulation is therefore extracted from equation 26. This gives a value of $\gamma_{DEM} = 90.6mJ/m^2$. The simulations for drill bits V1 and V4 penetrating at 10 mm/s are now run with this $\Delta\gamma$ value and compared to the simulations run in the validation study from chapter 4.3. The results are shown in Figure 36 below.

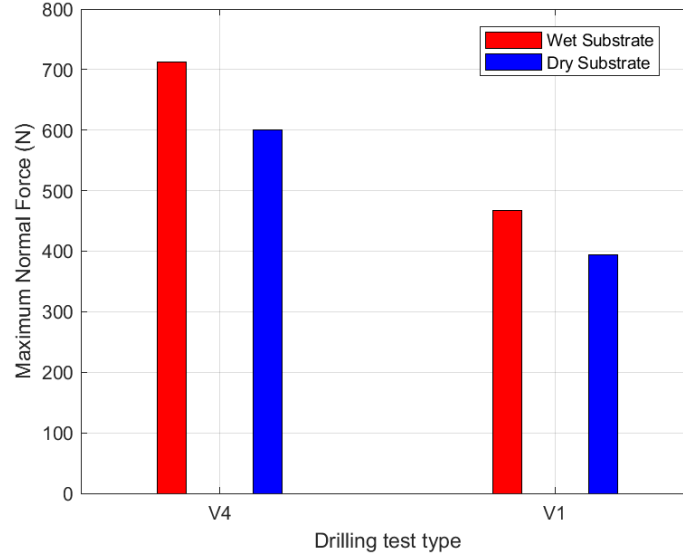


Figure 36: Comparison of simulation results for wet and dry substrate

The presence of higher adhesion forces, which in this case mimic the effects of capillary forces between the particles, has caused an increase in the necessary drilling force to penetrate the substrate. The results for the wet substrate are then extrapolated for the correct particle size and compared further to the experimental results obtained in Chapter 3. The comparison is presented in Table 5 below.

	V4	V1
Experiment result	24.3 N	15.6 N
Simulation result	712 N	467 N
Extrapolated result	16.8 N	10.9 N

Table 5: Comparison between simulation and experiment results of adhesion tests

From Table 5 it becomes clear that, while a JKR adhesion approximation for capillary forces did increase the normal force, it did not achieve a high enough increase in force demonstrated in the experiments. This is due to the fact that JKR adhesion model in DEM takes into account only the spheres that are in direct physical contact with each other. In real life, capillary forces can form contacts via capillary bridges even if they are not in direct contact with each other. This means that the current model omits many contacts between the spheres of the substrate. To circumvent this obstacle, on a trial and error basis, it was determined that an inflated value of $\Delta\gamma = 1040mJ/m^2$, will produce almost the exact values of the experimentally determined normal force, and shall be used further with this model to analyze the effects of capillary forces on drilling.

5 Results and discussion

This chapter presents and discusses the findings from the Discrete Element Method simulations conducted to investigate the effectiveness of reciprocating drilling compared to conventional penetration and rotational drilling methods. The primary objective of this study is to evaluate the performance differences between these drilling techniques, focusing on metrics such as the normal force.

The results are analyzed to provide insights into the mechanical interactions between the drill bit and the glass sand in a similar manner to that of the conducted experiments, highlighting the advantages and limitations of each method. By comparing the data from the simulations, the most effective drilling performance is determined in terms of the maximum normal force applied during drilling. The results obtained through simulations are further discussed and analyzed to improve the understanding of the outcomes. Ultimately, this chapter seeks to contribute to a deeper understanding of how different drilling methods behave, with the goal of optimizing future drilling technologies.

5.1 Comparing different drilling methods

The simulations for each drilling motion were run and the results of the maximum normal forces exerted on the drill are summarized in Figure 37 below. The input parameters of these simulations are summarized in Table 6. These input parameters are derived such that the input actuation power is similar for all drilling cases, this will be discussed further in Chapter 5.2.

Parameter	Value
v_1 - penetration speed at pure penetration	2.41 m/s
v_2 - penetration speed at rotation	2.38 m/s
ω - angular velocity	3.14 rad/s
v_3 - penetration speed at reciprocation	1.21 m/s
f - reciprocating frequency	60 Hz

Table 6: Input parameters for drilling motion comparisons at $f=60$ Hz

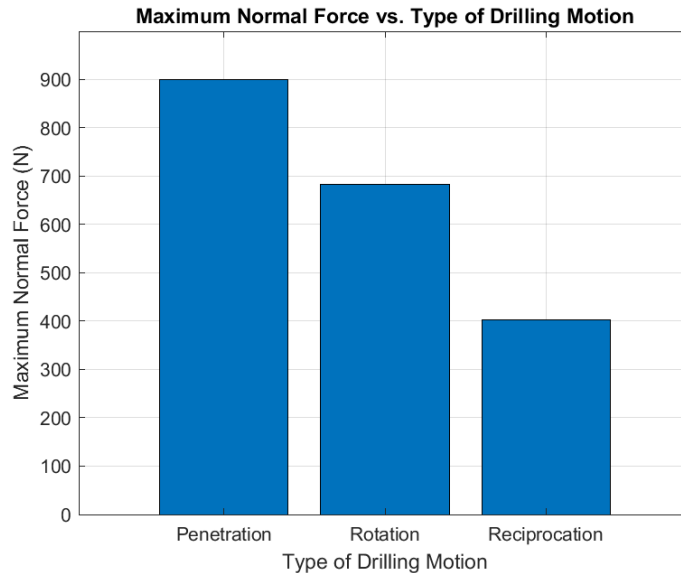


Figure 37: Maximum normal force for different drilling methods at $f=60$ Hz

The results obtained from the simulations show that adding either rotation or reciprocation into the system will reduce the normal force during drilling compared to penetrative drilling. It is also shown that during reciprocation the drill bit experiences a smaller normal force than during rotational drilling. These results are obtained at the reciprocation frequency of 60 Hz. A decision is made to investigate the effect of reciprocation frequency on the normal force during drilling. The results are displayed in Figure 38 below.

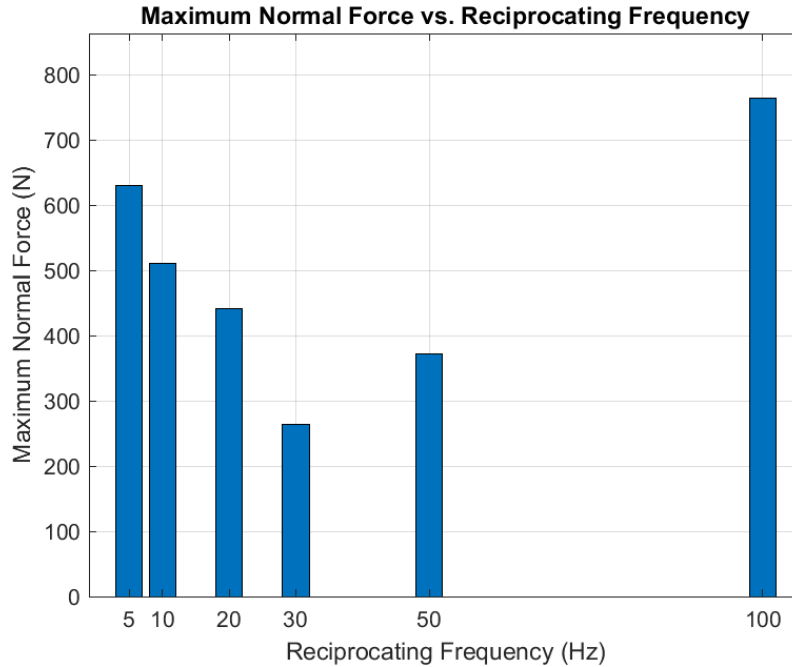


Figure 38: Maximum normal force for different reciprocation frequencies

It becomes clear that reciprocation drilling has a range of values in which the normal force is at its lowest, while that force significantly increases outside of that optimal range. A reciprocation frequency of about 30 Hz shows the most advantageous maximum normal force. Therefore, a comparison is made between the different drilling motions again, but this time the frequency is constrained to 30 Hz. The simulations were run once again and the results are displayed in Figure 39, and the input parameters for these simulations are summarized in Table 7.

Parameter	Value
v_1 - penetration speed at pure penetration	2.41 m/s
v_2 - penetration speed at rotation	2.38 m/s
ω - angular velocity	3.14 rad/s
v_3 - penetration speed at reciprocation	1.82 m/s
f - reciprocating frequency	30 Hz

Table 7: Simulation parameters for constrained $f=30$ Hz

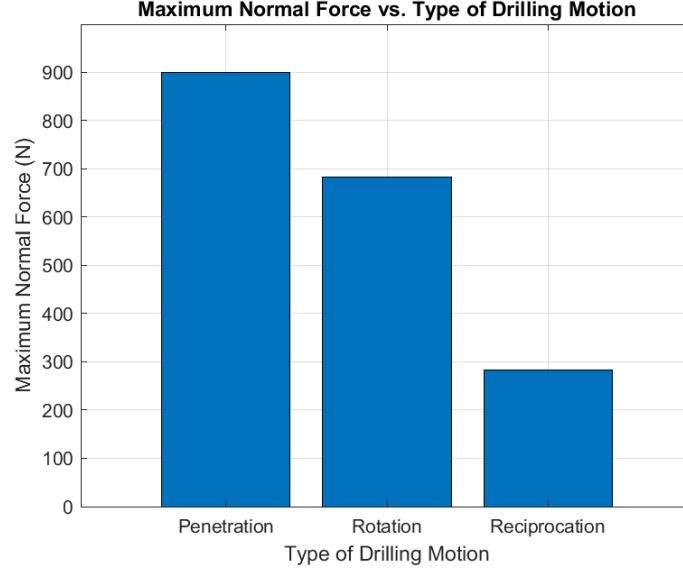


Figure 39: Maximum normal force for different drilling methods at $f=30$ Hz

This clearly shows that the normal force further reduces for reciprocating drilling at $f = 30\text{Hz}$. This concludes that dual reciprocation shows promising results in the range of about 25-35 Hz. This is an interesting result that is analyzed further by looking at the coordination number and the contact forces between the particles of the substrate in sections 6.3 and 6.4.

5.2 Power analysis

The goal of the simulations included in this study is to compare the different drilling methods and determine which one is the most effective when it comes to lowering the drilling force. In the case of penetrative drilling, the drill only needs to do work to penetrate the substrate vertically, while in the rotating motion, the drill has to penetrate the substrate vertically but also rotate. If all three cases penetrated the substrate with the same speed, the rotating drill would use more power as it would also need to rotate and the reciprocating drill would need added power to facilitate reciprocation. This would make it difficult to determine which drill bit performs better, as one could argue that lower normal forces do not make a drilling motion better if it ends up consuming more power. This is why rotational drilling and DRD were assigned smaller penetrating speeds. It is necessary to check the power consumption of the three cases outlined in Figure 39, to conclude whether a correct selection of parameters was made by assessing if the power usage between the drills is similar.

For penetration drilling, a force-displacement graph was plotted as shown in Figure 40, the area under this graph represents the work done during the penetration of the drill bit. This information is used, together with the duration of drilling, to calculate the power consumption.

$$P = \frac{W}{t} = \frac{9.02[J]}{0.02747[s]} = 328.44[W] \quad (27)$$

The same method is used to compute the power used during rotation. In this case, the work done is calculated in two stages. Work done during the penetration of the drill is done using the force-displacement graph as shown in Figure 41. work required to rotate the drill is calculated from the Torque and angular displacement of the drill represented in Figure 42.

$$P = \frac{W}{t} = \frac{6.56 + 0.07[J]}{0.0210084[s]} = 315.77[W] \quad (28)$$

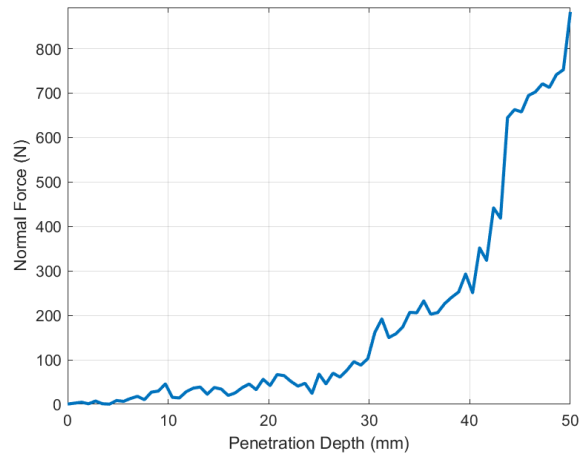


Figure 40: Force-displacement graph for penetration drilling

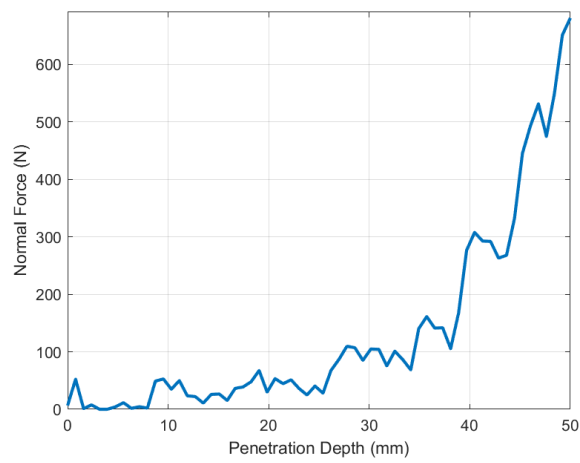


Figure 41: Force-displacement graph for rotational drilling

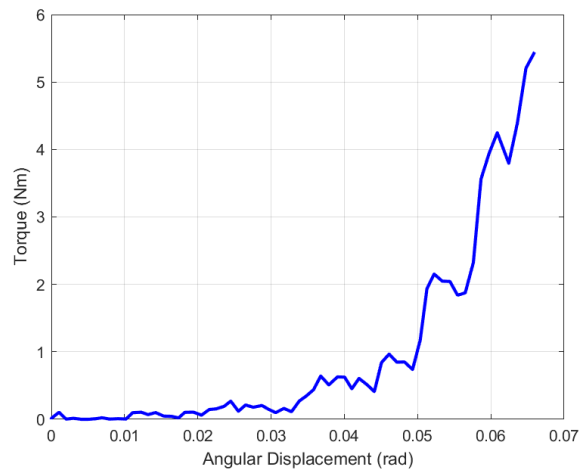


Figure 42: Torque-angular displacement graph for rotational drilling

Torque is calculated as a function of the forces acting on the drill bit and the varied radius of the tool as it penetrates. Since the simulation tracks all the normal components of the forces, the torque graphs resemble the normal force graphs in shape.

In the case of reciprocating drilling, the Force-displacement graph is used to determine the work done during penetration and reciprocation, as shown in Figure 43.

$$P = \frac{W}{t} = \frac{6.10[J]}{0.020747[s]} = 294.10[W] \quad (29)$$

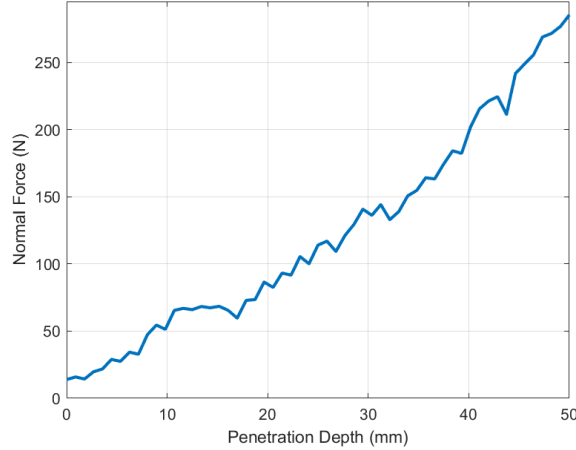


Figure 43: Force-displacement graph for reciprocating drilling

The force-displacement graphs of penetrative and rotary drilling show a small initial force which then sharply increases. In reciprocating drilling, the forces are slightly higher from the beginning and continue to increase steadily. In the first two cases, the contact area between the drill bit and the substrate is quite small due to the conical shape of the drill. In the reciprocating case, the downward stroke of the reciprocating motion creates a larger contact area with the substrate from the get-go. Additionally, the premise of reciprocating drilling is the repeated motion of downward and upward strokes which creates repeated impacts with the soil that can raise the overall force. Each downward stroke can further compress and compact the substrate, further increasing the forces at the early stages of drilling. Another explanation for this trend could be that conventional methods push more material outwards from the drilling site, this is especially true for rotation. In reciprocating drilling, the material removed in the oscillatory motion could stay stacked around the drilling site.

From equations 27, 28, and 29 it can be seen that the three drilling motions used approximately a similar amount of power, making them more suitable for comparisons of the normal forces. This power analysis concludes that for a similar power consumption, reciprocating drilling results in the smallest amount of normal force.

5.3 Substrate particle contact force distribution analysis

An adaptation to the code is made to export O.interactions between the ids of the glass particles. A condition is made to only export the interactions that result in a contact and they have to be sphere-to-sphere contacts. The engine is run every 100 iterations and compiles a list of contact forces between particles. The list is sorted to allocate a frequency for repeating values up to 3 decimal places. To easily understand the large dataset, histograms are made for small ranges of contact force values. A certain distribution model had to be fitted to the histogram data to better understand the spread of the force data. In granular systems, contact forces are often expected to follow a Rayleigh distribution, stemming from the triaxial shear tests, where force chains form in a quasi-static or slowly sheared system [15]. In such cases, the Rayleigh distribution captures the variance in force magnitudes, with most forces being small and well-distributed and only a few larger force chains bearing the load. Based on this understanding, a similar distribution was expected in these drilling simulations. However, the contact force data seemed to be distributed with a log-normal method. This could be explained by the dynamic nature of the drilling process, which involves particle impacts and rapid grain rearrangements that add more variability to the system. These transient processes often result in a log-normal distribution, with most occurrences

near the lower end with some extreme outliers [38]. This force concentration seemingly follows the data trends gathered in the contact force analysis.

A log-normal distribution is fitted to each histogram to model the underlying distribution of contact forces. The histogram represents the observed frequency percentages for different force intervals (0.005 N bin width), and the log-normal curve provides the distribution of force magnitudes. The log-normal distribution is a continuous probability distribution of a random variable whose logarithm is normally distributed. The log-normal distribution is fitted to the frequency data by first estimating the shape and scale parameters, using a maximum likelihood estimation (MLE) or fitting process based on the natural logarithms of the data. The log-normal distribution is characterized by its positively skewed shape, which means it has a long right-hand tail. The probability density function (PDF) of the log-normal distribution is given by:

$$f(x; \mu, \sigma) = \frac{1}{x\sigma\sqrt{2\pi}} e^{-\frac{(\ln x - \mu)^2}{2\sigma^2}} \quad (30)$$

where x is the contact force, μ is the mean of the logarithm of the contact forces and σ is the standard deviation.

This function is computed and scaled to match the total frequency counts and the bin width, ensuring the area under the curve aligns with the observed data. Finally, the fitted distribution is plotted alongside the empirical frequency data for each case, allowing for a visual comparison that illustrates how well the log-normal model describes the distribution of contact forces. Figure 44 represents the distribution of particle contact forces at a reciprocation frequency of 10 Hz, while Figure 45 and Figure 46 show the results for 30 Hz and 100 Hz respectively. A comparison between these three values will provide further insight into the effects of varying the reciprocating frequency on the outcome of the maximum normal force during reciprocating drilling.

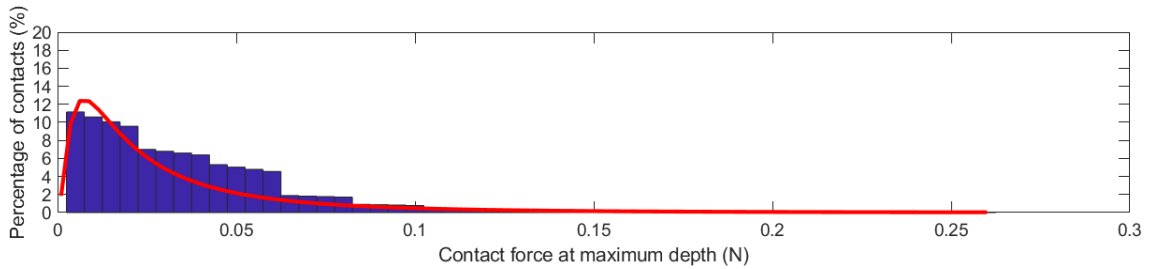


Figure 44: Particle contact force distribution at $f=10$ Hz

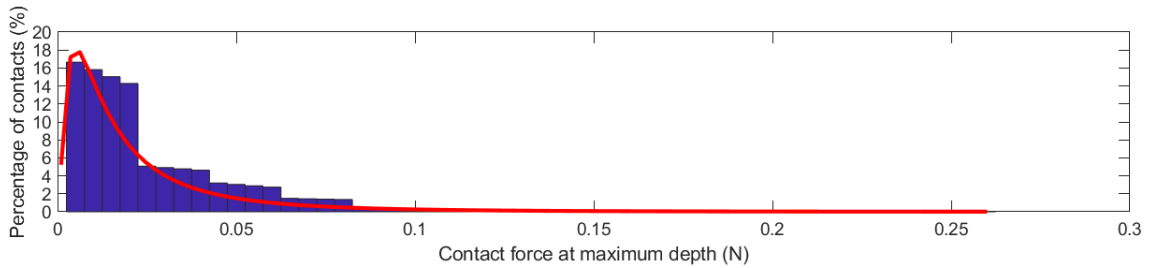


Figure 45: Particle contact force distribution at $f=30$ Hz

It is observed that for $f = 30Hz$, which yields the lowest normal force during drilling, contact force distribution is the narrowest with the highest distribution peak, while for $f = 100Hz$, the contact forces are better distributed. This further supports the results displayed in Figure 38, as granular beds experience increased particle jamming when the contact forces are more distributed, and there is increased stability of force chains due to less stress localization. The contact forces are considered well-developed if they are more distributed across different values [16]. These results are

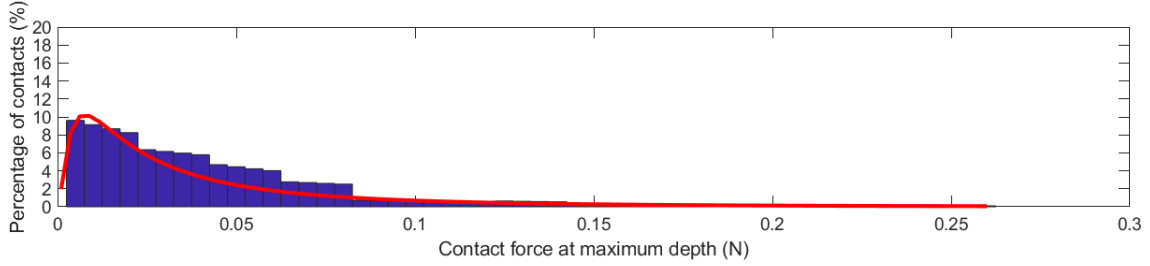


Figure 46: Particle contact force distribution at $f=100$ Hz

also supported by the research of Alkalla, introduced in Chapter 2 ([2] [3]). His research concluded that particle interlocking or jamming has the most effect on toothed reciprocating drills and that the overall success of DRD depends on its ability to fluidize the regolith. This research further pin-points this ability to fluidize the regolith and reduce particle jamming to a specific parameter of DRD - the reciprocating frequency.

To further analyze the comparison between rotational and reciprocating drilling, the contact force distribution of the rotating drilling example from Figure 39 is shown in Figure 47 below. According to the normal force data gathered, this method performs better than DRD at $f = 100Hz$, while it is outperformed by both DRD at $f = 30Hz$ and $f = 10Hz$. Given this, the contact force distribution is expected to be less distributed than in the $f = 100Hz$ case, but more distributed than in the $f = 30Hz$ and $f = 10Hz$ cases. This was demonstrated, as the distribution was slightly broader with a lower peak than that of $f = 10Hz$, yet much narrower with a peak higher than that in the $f = 100Hz$ case. This concluded that in the cases shown earlier in Figure 39, reciprocating drilling at $f = 30Hz$ creates less developed force chains in the substrate, making it easier to penetrate soil than its rotating counterpart.

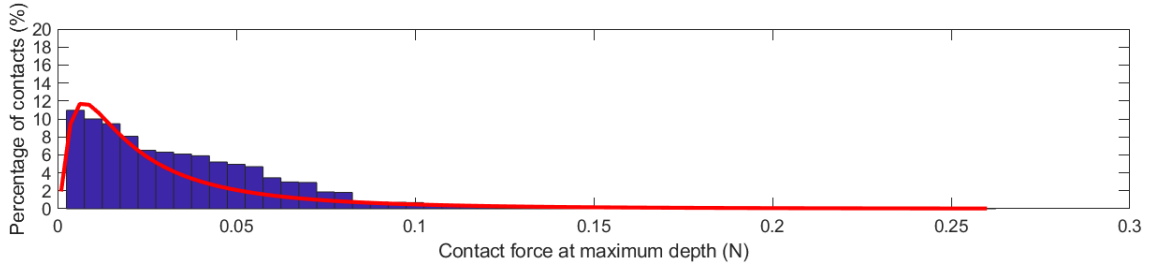


Figure 47: Particle contact force distribution for rotation

5.4 Coordination number analysis

To further explain the trends observed in Figure 39, a comparison between the different coordination numbers is made. At maximum penetration depth, the coordination number for reciprocating drilling is around 1.52, while rotation and penetration have the value of Z equal to 3.91 and 4.92 respectively. This is visualized in Figure 48 below. According to Silbert [34] a higher value of the coordination number, represents a more stable system. The more stable the granular system is, the more it becomes difficult to penetrate it, resulting in higher drilling forces being observed. A similar trend is observed when comparing the coordination number of simulations with a varying reciprocation frequency. The low force system ($f = 30Hz$), as stated earlier, has Z equal to 1.52, while drilling systems experiencing higher normal forces ($f = 10Hz$ and $f = 100Hz$) have Z equal to 3.54 and 4.41 respectively. As the actuation process in the drilling mechanism increases, such as through higher frequencies or more complex movements, the degrees of freedom of the particles in the granular bed also increase. This increase in degrees of freedom allows the particles to move more freely and become less constrained. As a result, the coordination number decreases. A lower coordination number indicates a less stable system with fewer inter-particle connections, which makes the granular bed more prone to particle rearrangements and shifts during drilling. Higher values of Z , particularly values higher than 4, characterize a particle system where jamming is highly present.

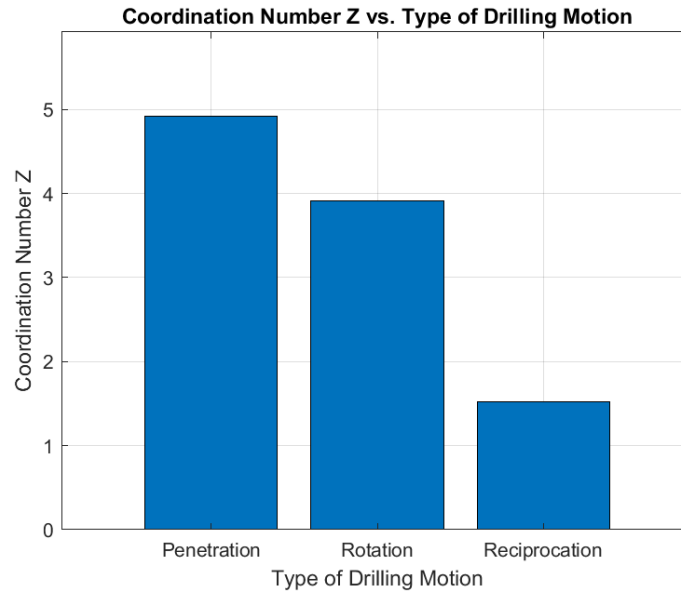


Figure 48: Coordination number for different drilling motions

5.5 Modelling limitations and challenges

It is important to additionally address certain limitations to the numerical model used during this study. For example, in the numerical model, it is virtually possible to infinitely increase the reciprocation frequency without introducing large vibrations into the system. In real-world applications it is likely that with increasing values of f the drill bit will start to vibrate or oscillate in the horizontal direction. The rapid oscillations cause instability in the drill bit, resulting in erratic contact with the substrate at inadequate angles. This many poor contacts between the drill bit and the substrate increase resistance and generate higher normal forces, making the drilling process more difficult and less effective. Understanding how these vibrations will affect the optimal frequency range for reciprocation drilling will provide further confidence in the results gathered in this study.

Furthermore, the focus of this study heavily relied on normal force computation, while there are other drilling forces and parameters that are necessary to consider before a final ruling can be made on the effectiveness of reciprocation drilling. Tool wear and failure modes were not considered. For example, in coarser substrates, the reciprocating drill is more likely to fail, as particles can become stuck between the two reciprocating halves and grind down the drill during reciprocating strokes. This type of failure is not as relevant for a solid, rotating drill. Overall, the material selection and lifecycle considerations for the drilling tool material should also play a role in the choice of drilling mechanisms.

Other parameters that can influence drilling need to be addressed. For example, temperature considerations and heat generation were not involved in the DEM study. Drilling is also dependent on the rate of material removal from the bore. This parameter was also not researched in the context of reciprocating drilling and its efficiency. To truly compare the performance of different drilling mechanisms, it is necessary to test them in more life-like scenarios, which this study lacks. The substrate used during this entire research consisted of perfect, smooth, glass spheres of equal diameter. In reality, the soil is far more coarse, heterogeneous, and overall complex with pore fluids and uneven particle sizes present.

Finally, the method of approach to DEM simulations itself can be discussed. In this study, a choice was made to compare simulations to experiments. Simulations were assigned as many realistic parameters as possible and the results were recorded. During the course of this research, it became apparent that this is not the best approach to DEM and YADE simulations in particular. The bulk behavior of granular materials is difficult to represent with simple point contacts and other simplifications, and computational complexity poses challenges to maintaining realistic conditions at all times. A more common approach is to not use realistic values for certain properties, but

manipulate them until simulation results match those of the experiments [6].

From a wider perspective, the findings of this study have important implications for real-world drilling applications, particularly in optimizing drilling efficiency and tool performance. The demonstrated benefits of reciprocating drilling, with its ability to significantly reduce normal forces, suggest that integrating reciprocation into drilling systems could improve operational performance, especially in challenging rock formations. However, the sensitivity of reciprocation drilling to frequency highlights the need for careful calibration of drilling parameters. Operators would need to balance reciprocation frequency to avoid adverse effects of high-frequency vibrations, which can increase normal forces and reduce efficiency. Ultimately, this study provides a foundation for advancing drilling methods to improve energy efficiency, reduce tool wear, and enhance overall drilling success in complex environments. Furthermore, this study also contributes to advancing research into bio-inspired drilling technologies, specifically dual reciprocation, which can lead to more sustainable drilling practices by enhancing efficiency and reducing environmental impact.

6 Conclusion and recommendation

6.1 Conclusion

This research set out to evaluate the effectiveness of reciprocating drilling compared to conventional rotational drilling, focusing on how these methods perform under various conditions and examining the potential advantages of bio-inspired technologies. Through a series of experiments and numerical simulations, this study aimed to identify key factors influencing the performance of these drilling techniques and lay the groundwork for future research.

- First, a set of already existing penetration drilling experiments was checked for repeatability. Once the integrity of the experimental setup was confirmed, additional experiments confirmed that adding rotation to the drilling system had reduced the normal force during drilling. On the contrary, it was found that introducing moisture into the system significantly increased the normal force. Since it was not possible to carry out experiments with the dual reciprocating drill, a numerical model was developed.
- A scaled-down test model was used to check the conformity of the model to the theoretical background which revealed expected trends. Increasing the coefficient of friction, elastic modulus, and introducing adhesion and capillarity into the system all resulted in increased normal forces during drilling. Increasing the penetration speed had no effect on the normal force recorded, which was also observed in the experiments. This was further investigated by looking at the coordination number at different drilling speeds. At sufficiently low speeds, it was found that the coordination number did not vary much, showing that there were no significant changes to the stability and connectivity of the granular bed. At sufficiently high speed, the disruptions in the granular bed would eventually cause the normal force to rise.
- Since the real particle size in the full-sized domain was impossible to simulate, given the current computational power, a further study into the particle size of the substrate revealed that increasing the particle size would increase the normal force. This relation was later used to extrapolate the force results at increased particle sizes, which made the real-scale simulations possible.
- Three simulation results were then compared to the results of their experimental counterparts to further validate the integrity of the model. Since the results were within 15% of each other, the model was deemed functional.
- The model was expanded to describe dual reciprocating motion. Simulations were run for three different types of drilling motion: penetration, rotation, and reciprocation, and their results had to be compared to determine which drilling mechanism delivered the lowest normal force. Power requirements for each case were analyzed to conclude whether the chosen simulation parameters produced similar power requirements for all three cases. The power used by all three drills was similar.
- Comparisons showed that rotating drilling outperformed penetrative drilling, and that reciprocation outperformed rotation. Further studies into the frequency of reciprocation determined that reciprocating drilling has a set frequency range of about 25-35 Hz in which it outperforms other methods the most. Outside of this frequency range, the benefits of reciprocation are slowly diminished.
- The results obtained support the previous research on DRD done by M. Alkalla in which he concluded that the performance of reciprocating drilling depends on the drill motion's ability to fluidize the substrate and that for the toothed DRD drill bits, particle jamming, and interlocking becomes the limiting factor.

These results can be used to successfully answer the pre-imposed research question and sub-questions that shaped this study:

- **Can the DEM simulation be validated against simple penetration experiments?**
 - Yes, the numerical model was able to reproduce experimental results with less than 15% error, providing confidence in its accuracy for further analysis.
- **Can DEM be used to model dual reciprocation motion?**
 - Yes, model updates were made to incorporate a time-dependent sinusoidal function, enabling the simulation of dual reciprocation motion.
- **Can penetration forces of different drilling methods be compared?**
 - Yes, since the power used in all three cases is similar in value, the different drilling motions can be compared based on their normal force values.
- **Is reciprocating drilling more effective than rotational drilling?**
 - This research indicates that reciprocating drilling is more effective than rotational drilling, as measured by the magnitude of the normal force exerted on the drill bit during drilling. Lower normal force values are favorable, and the findings suggest that dual reciprocation achieves significantly lower normal forces compared to its rotational counterpart. The effectiveness of reciprocating drilling depends on specific operational parameters, particularly the reciprocating frequency. Outside of the optimal parameter range, reciprocating drilling may lose its advantages over other methods. The study emphasizes the importance of carefully tuning these parameters to fully exploit the benefits of reciprocating drilling. However, as mentioned in Chapter 5.5, normal force is only one parameter in a complex system. Looking further into rates of material removal, further force analysis, wear and failure modes research should also be assessed before a definitive conclusion can be made.

In summary, this study not only demonstrated the potential for dual reciprocation in drilling applications but also provided a foundation for future research into bio-inspired drilling technologies. With further refinement and optimization, these advancements hold the promise of revolutionizing drilling processes, enhancing efficiency, and reducing environmental impact in the industry.

6.2 Recommendation

To aid the advancement of bio-inspired drilling technologies and further complement the outcomes of this study, more research is necessary in certain key areas:

- Understanding and optimizing reciprocating frequency is essential for achieving optimal performance of the reciprocating drill. Detailed studies should be conducted to identify the specific conditions under which reciprocating drilling outperforms conventional methods, to solidify the frequency range to be used by the drills. This testing should incorporate the effects of unwanted vibrations with the rising reciprocation frequency, introduced in Chapter 5.4.
- It is necessary to compare the different drilling mechanisms from various points of view. For example, performing a failure modes and effects analysis on each type of drill, life cycle analysis, material selection or rate of material removal may come to a different conclusion regarding the efficacy of a reciprocating drill.
- To further strengthen the model in question, adapting its parameters to fit the real world more closely can bring more accuracy. Taking into account heat generation, drill lubrication, or conducting experiments to closely determine the values of the coefficient of friction and stiffness of the glass beads, will bring the simulation a step closer to reality. As mentioned before, it is also necessary to focus on developing more realistic soil models in DEM. The type

of soil is an important factor in drilling and determining which types of soil reciprocating drilling outperforms other methods in is crucial.

- Considering different approaches to DEM simulations is also a possible research route due to the computational complexity of the task. Modeling life-like parameters can be difficult with limited computing power, which is why further optimizations and extrapolations can be considered. As mentioned in Chapter 5, fitting the parameters of the numerical model, such that the outputs closely match the experimental results, is a common approach in DEM that can be explored further for this application.
- The definitive next steps would be to facilitate for experimental testing with the DRD setup in the laboratory at the University of Twente, to see whether similar trends are observed. This can be done through the addition of sensors and minimizing current frictional losses in the system. Additionally, up-scaling the numerical model can be useful to test reciprocating drilling in an industrial setting. Rotary drills, which currently dominate the industry, are many times larger than the model tested with the current simulations. It is beneficial to investigate whether the reciprocating drill still delivers the same results at much larger scales, to gain insight into its applications within the industry.

In the bigger picture, another important avenue is the development of more new bio-inspired drill bits and materials. Research should explore how these innovations can be designed and tested to improve drilling performance and durability. Assessing the environmental impact of these new technologies is vital to ensure that they offer sustainable solutions. Additionally, conducting comprehensive cost-benefit analyses will help evaluate the economic feasibility of implementing these advanced methods on a larger scale. Field trials are necessary to validate theoretical models and simulations in real-world conditions. These trials should be complemented by interdisciplinary collaboration among engineers, biologists, and industry professionals to bridge the gap between theoretical research and practical application. Such collaborations can facilitate the development of innovative solutions and accelerate the adoption of new technologies. By addressing these areas, future research can drive significant advancements in drilling technology, leading to improved performance, efficiency, and sustainability in the industry.

References

- [1] Ohio Environmental Protection Agency. “Drilling and Subsurface Sampling”. In: (October 2017).
- [2] Mohamed Alkalla, Yang Gao, and Arthur Bouton. “Customizable and Optimized Drill Bits Bio-inspired from Wood–Wasp Ovipositor Morphology for Extraterrestrial Surfaces*”. In: July 2019, pp. 430–435. DOI: 10.1109/AIM.2019.8868816.
- [3] Mohamed Alkalla et al. “DROD: A hybrid biomimetic undulatory and reciprocatory drill: Quantitative analysis and numerical study”. In: *Acta Astronautica* 182 (Feb. 2021). DOI: 10.1016/j.actaastro.2021.02.007.
- [4] Ardalan Amiri. “Investigation of Discrete Element and Bonded Particle Methods for Modelling Rock Mechanics Subjected to Standard Tests and Dual Reciprocating Drilling”. PhD thesis. Sept. 2017. DOI: 10.13140/RG.2.2.35823.56482.
- [5] Vasileios Angelidakis et al. “YADE - An extensible framework for the interactive simulation of multiscale, multiphase, and multiphysics particulate systems”. In: *Computer Physics Communications* 304 (2024), p. 109293. ISSN: 0010-4655. DOI: <https://doi.org/10.1016/j.cpc.2024.109293>. URL: <https://www.sciencedirect.com/science/article/pii/S0010465524002169>.
- [6] Vasileios Angelidakis et al. “YADE - An extensible framework for the interactive simulation of multiscale, multiphase, and multiphysics particulate systems”. In: *Computer Physics Communications* 304 (2024), p. 109293. ISSN: 0010-4655. DOI: <https://doi.org/10.1016/j.cpc.2024.109293>. URL: <https://www.sciencedirect.com/science/article/pii/S0010465524002169>.
- [7] A. Aryee. “Risks of Offshore Oil Drilling: Causes and Consequences of British Petroleum Oil Rig Explosion.” In: *Aquatic Science and Technology* (2012).
- [8] Hans-Jürgen Butt and Michael Kappl. “Capillary Forces”. In: Apr. 2018, pp. 131–166. ISBN: 9783527341658. DOI: 10.1002/9783527804351.ch5.
- [9] Black Diamond Drilling Co. *History of Drilling*. Accessed: November 2023. 2023. URL: <https://www.bddrill.ca/drilling-school/history-%20of-drilling/>.
- [10] Alberto Cuitiño et al. “Experimental characterization of the behavior of granular visco-plastic and visco-elastic solids during compaction”. In: *Journal of Materials Science* 36 (Nov. 2001), pp. 5487–5495. DOI: 10.1023/A:1012450221092.
- [11] Esimtech. *Understanding Conventional Rotary Drilling*. Accessed: November 2023. URL: <https://www.esimtech.com/understanding-%20conventional-rotary-drilling-pros-cons-and-what-are-its-alternatives.html>.
- [12] E. Gordon J. *Structures*. Da Capo Press, 1978.
- [13] Thibault Gouache et al. “Wood Wasp Inspired Planetary and Earth Drill”. In: Mar. 2010. ISBN: 978-953-307-025-4. DOI: 10.5772/8775.
- [14] K. He. “Seismic dynamics of offshore wind turbine-seabed foundation: Insights from a numerical study”. In: *Renewable Energy* 205 (2023).
- [15] Shuling Huang et al. “Triaxial Test and Mechanical Analysis of Rock-Soil Aggregate Sampled from Natural Sliding Mass”. In: *Advances in Materials Science and Engineering* 2015 (Mar. 2015), pp. 1–14. DOI: 10.1155/2015/238095.
- [16] et.al. J. Hao. “Jamming in granular shear flows of frictional, polydisperse cylindrical particles”. In: *Advanced Powder technology* (2021).
- [17] F. Julian and V. Vincent. *The Mechanism of Drilling by Wood Wasp Ovipositor*. Vol. 03. 04. 1995.
- [18] T. Mishra K. Vink. “Enhancing the drilling performance of a bio-inspired reciprocating drilling setup through design modifications in the drill bit.” In: (2024).
- [19] Marcus King and Julian Vincent. “The mechanism of drilling by wood wasp ovipositors”. In: *Biomimetics* 3 (Jan. 1995), pp. 187–201.
- [20] Bogdan Kopey. “Development of Drilling Technics from Ancient Ages to Modern Times”. In: (Jan. 2007).
- [21] Vitázoslav Krúpa et al. “Measurement, modeling and prediction of penetration depth in rotary drilling of rocks”. In: *Measurement* 117 (2018), pp. 165–175. ISSN: 0263-2241. DOI: <https://doi.org/10.1016/j.measurement.2017.12.007>. URL: <https://www.sciencedirect.com/science/article/pii/S0263224117307789>.
- [22] O. Kuhn. *Ancient Chinese Drilling*. Vol. 29. 06. 2004.

- [23] Wan-Qing Li et al. “Comparison research on the neighbor list algorithms: Verlet table and linked-cell”. In: *Computer Physics Communications* 181.10 (2010), pp. 1682–1686. ISSN: 0010-4655. DOI: <https://doi.org/10.1016/j.cpc.2010.06.005>. URL: <https://www.sciencedirect.com/science/article/pii/S0010465510001827>.
- [24] Tianxi Liu et al. “Equivalent boundary model of lunar soil drilling simulation by DEM”. In: *Journal of Terramechanics* 91 (2020), pp. 85–95. ISSN: 0022-4898. DOI: <https://doi.org/10.1016/j.jterra.2020.06.003>. URL: <https://www.sciencedirect.com/science/article/pii/S0022489820300549>.
- [25] S. Luding and colleagues. “Understanding slow compression of frictional granular particles by network analysis”. In: *Soft Matter* 10 (2014), pp. 652–662. DOI: 10.1039/D4SM00560K.
- [26] Amitava Mukherjee. *Biomimetics, learning from Nature*. Intech, 2010.
- [27] et. al. Nallala S.C. “DEM analysis of small and small-to-medium strain shear modulus of sands”. In: *Computers and Geotechnics* (2021).
- [28] Craig Pitcher et al. “Development of the Third Generation of the Dual-Reciprocating Drill”. In: *Biomimetics* 5.3 (2020). ISSN: 2313-7673. URL: <https://www.mdpi.com/2313-7673/5/3/38>.
- [29] Valentin Popov and Markus Heß. “Tangential Contact”. In: Jan. 2015, pp. 65–86. ISBN: 978-3-642-53875-9. DOI: 10.1007/978-3-662-46160-0_5.
- [30] Valentin L. Popov. *Contact Mechanics and Friction*. Springer, 2010.
- [31] L. Quintero. *Developments in Surface Contamination and Cleaning*. 2013.
- [32] Loc Vu-Quoc and Xiang Zhang. “An accurate and efficient tangential force–displacement model for elastic frictional contact in particle-flow simulations”. In: *Mechanics of Materials* 31.4 (1999), pp. 235–269. ISSN: 0167-6636. DOI: [https://doi.org/10.1016/S0167-6636\(98\)00064-7](https://doi.org/10.1016/S0167-6636(98)00064-7). URL: <https://www.sciencedirect.com/science/article/pii/S0167663698000647>.
- [33] Aneta Sapińska-Śliwa et al. “Rotary - percussion drilling method - historical review and current possibilities of application”. In: *AGH Drilling, Oil, Gas* 32 (Jan. 2015), p. 313. DOI: 10.7494/drill.2015.32.2.313.
- [34] L.E. Silbert. “Jamming of frictional spheres and random loose packing”. In: *Soft Matter* (2010).
- [35] T. Spohn and et al. “The InSight-HP3 mole on Mars: Lessons learned from attempts to penetrate to depth in the Martian soil”. In: *Advances in Space research* 69.08 (2022).
- [36] Colin Thornton. *Granular Dynamics, Contact Mechanics and Particle System Simulations*. Springer, 2015.
- [37] et.al. U. cerkevenik. “Mechanisms of ovipositor insertion and steering of a parasitic wasp”. In: *PNAS* (2017).
- [38] Math Works. “Lognormal Distribution”. In: URL:<https://nl.mathworks.com/help/stats/lognormal-distribution.html> (Accessed: October 2024).
- [39] et.al. Xi Y. Yao Y. “Experiment study and numerical simulation on the dynamic rock-breaking process of rotary percussive drilling with different cyclic and stress-wave frequencies”. In: *Petroleum Science and Technology*, 42(23), 3497–3517 (2023).
- [40] YADE. “Manual and documentation”. In: ().
- [41] Jianjun Yang and E.G. Wang. “Reaction of water on silica surfaces”. In: *Current Opinion in Solid State and Materials Science* 10.1 (2006), pp. 33–39. ISSN: 1359-0286. DOI: <https://doi.org/10.1016/j.cossms.2006.02.001>. URL: <https://www.sciencedirect.com/science/article/pii/S1359028606000027>.
- [42] Z. Zhang. *Rock Fracture and Blasting - Theory and Applications*. Elsevier, 2016, pp. 155–175.